Viral Generation, Packaging, and Transduction on a Digital Microfluidic Platform

Angela Quach

A Thesis

in

The Department

of

Biology

Presented in Partial Fulfillment of the Requirements
for the Degree of Master of Science (Biology) at
Concordia University
Montreal, Quebec, Canada

September 2021

CONCORDIA UNIVERSITY

School of Graduate Studies

This is to certify that the thesis is prepared

By: Angela Quach

Entitled: Viral Generation, Packaging and Transduction on a Digital Microfluidic Platform

and submitted in partial fulfillment of the requirements for the degree of

Master of Science (Biology)

complies with the regulations of the University and meets the accepted standards with respect to originality and quality.

Signed by the final Examining Committee:

_____ Chair/Examiner

Dr. Alisa Piekny

_____ External Examiner

Dr. David Kwan

_____Examiner

Dr. Laurent Potvin-Trottier

_____ Supervisor

Dr. Steve Shih

Approved by _____

Chair of Department or Graduate Program Director

Date_____2021 _____

Dean of Faculty

ABSTRACT

Viral Generation, Packaging, and Transduction on a Digital Microfluidic Platform

Angela Quach

Viral-based systems are a popular delivery method for introducing exogenous genetic material (e.g., plasmids or shRNA) into mammalian cells. In particular, virus-like particles have shown to be efficient, in packaging large vectors and complexes (e.g., Cas 9) and in their delivery into cells via entry mechanisms of an enveloped virus particle. Unfortunately, the preparation and packaging of virus-based particles containing the machinery to edit the cells is labour-intensive, with many steps requiring optimization and sensitive handling. Furthermore, following packaging, is delivering the viral particles efficiently into the desired cell line, which can vary significantly between cell lines since different cells uptake the virus at different rates. In recognition to these challenges, we introduce the first microfluidic method that integrates lentiviral generation, packaging, and transduction. The new method allows for the production of viral titers between 10^6-10^7 (similar to macroscale production) and high transduction efficiency for hard-to-transfect cell lines. To extend the technique to be useful for gene-editing applications, we show how this technique can be used to knockout and knockdown estrogen receptor gene – a gene prominently responsible for 70% of breast cancer cases. This new technique is automated with multiplexing capabilities, which have the potential to standardize the methods for viral-based genome engineering.

This thesis is dedicated to my parents for having supported me throughout this endeavour and for giving me all their love unconditionally.

Acknowledgements

I would like to thank Dr. Sylvie Mader and her former student Dr. Justyna Kulpa for fruitful discussions on lentiviral packaging and transduction. We also thank Dr. Chris Law for microscope training at the Center for Microscopy and Cellular Imaging (CMCI). In addition, we thank Dr. David Walsh for access to the PCR system. Moreover, we thank Hugo Sinha (DropGenie) and Kevin Larocque (Dr. Piekny lab) for cell culture and gene editing advice. We thank Dr. Smita Amarnath from the Genome Foundry for training with the flow cytometer machine. I would like to give a special mention to each of my labmates for always being helpful and encouraging towards me. I would also like to thank my supervisor Dr. Steve Shih for continuously being patient with me and for pushing me to through challenges that I thought I could not overcome. I would like to thank the personnel at the Martin lab for being resourceful and giving me tips when I needed advice. We thank the Natural Sciences and Engineering Research Council (NSERC) (including the SynBioApps CREATE program), the Fonds de Recherche Nature et technologies (FRQNT), MEDTEQ+, and the Canadian Foundation of Innovation (CFI) for funding. SRL thank NSERC for a CGS scholarship and Concordia University Department of Electrical and Computer Engineering for FRS Funding. SCCS thanks Concordia for a University Research Chair.

Overview of Chapters

This thesis describes the project I conducted and completed for my Master's in Science in Dr. Steve Shih's research group at Concordia University. In this work, I introduce an automated digital microfluidics platform for lentiviral generation, the packaging, production, and transduction of lentiviruses in target cells for gene disruption. This thesis starts with a short review on the theory of gene editing and gene regulation, challenges associated with viral generation, exploration of different microfluidic paradigms with an emphasis on digital microfluidics, and a special focus on established microfluidic devices for lentiviral transduction. Furthermore, I will state my objectives and describe the methodology and the results obtained from the characterization and validation lentiviral experiments accomplished on the device and on benchtop.

Chapter 1 introduces several topics pertaining to my research project such as gene disruption techniques, the field of microfluidics and my objectives.

Chapter 2 describes the methodology utilized both on the microscale and macroscale side of the biological processes performed and validation methods for data compilation.

Chapter 3 discusses results in characterizing and validating the lentiviral generation platform. I will describe the device optimization, the characterization of the platform for lentiviral generation, the proof-of-concept of knocking out an endogenous fluorescent reporter in a lung cancer cell line and the validation work for knocking out and knocking down a receptor in a breast cancer cell line.

Chapter 4 presents concluding commentary concerning my work and a future perspective for microfluidics and gene disruption combined.

Overview of Author Contributions

The work presented here was made possible with the help of my colleagues in the Shih Lab. I will summarize the input that each other has contributed here.

The project was thought out and designed by myself, the research article relevant to this work was written and edited by myself and Dr. Steve Shih.

All experiments were performed by myself and I gathered and analyzed the data relevant to my thesis. The resulting figures were revised and edited by myself and Dr. Steve Shih.

Device fabrication and optimization was performed with the guidance of Samuel Little (PhD candidate).

The code for the automation system was written, optimized and troubleshooted by Guy Soffer. The hardware for the automation system was designed and optimized by Amin Firouzeh and Philippe Vo.

Table of Contents

List of Figures

List of Tables

List of Equations

List of Abbreviations

1. Clustered Regularly Interspaced Short Palindromic Repeats (CRISPR)
2. Colony-forming unit (CFU)
3. Computer-aided design (CAD)
4. CRISPR-associated (Cas)
5. Deionized (DI)
6. Digital microfluidic (DMF)
7. Dulbecco's modified eagle medium (DMEM)
8. Electrowetting-on-dielectric (EWOD)
9. Enhanced GFP (eGFP)
10. Estrogen receptor alpha (ERα or ESR1)
11. Extracellular signal-regulated kinase (ERK)
12. Fluorescent activated cell sorting (FACs)
13. Fetal bovine serum (FBS)
14. Green fluorescent protein (GFP)
15. Homology-Directed Repair (HDR)
16. Indium tin oxide (ITO)
17. Lentiviral generation (LENGEN)
18. Lysogeny broth (LB)
19. Mitogen-activated protein kinase (MAPK)
20. Multiplicity of infection (MOI)
21. Non-homologous end joining (NHEJ)
22. Phosphate buffer saline (PBS)
23. Polymerase chain reaction (PCR)
24. Printed circuit board (PCB)
25. Quantitative real-time polymerase chain reaction (qRT-PCR)
26. RNA interference (RNAi)
27. RNA-induced silencing complex (RISC)
28. Roswell Park Memorial Institute (RPMI)
29. Short hairpin RNA (shRNA)
30. Single guide RNA (sgRNA)
31. Small interfering RNA (siRNA)
32. Transcription activator-like effector nuclease (TALEN)
33. Transducing unit (TU)
34. Tris-acetate-EDTA (TAE)

List of Co-Authored Publications

An Automated Microfluidic Gene-Editing Platform for Deciphering Cancer Genes

Hugo Sinha[1,2], **Angela B.V. Quach[2,3]**, Philippe Q.N. Vo[1,2], Steve C.C. Shih[1-3]

[1]Department of Electrical and Computer Engineering, Concordia University, Montréal, Québec, Canada
[2]Centre for Applied Synthetic Biology, Concordia University, Montréal, Québec, Canada
[3] Department of Biology, Concordia University, Montréal, Québec, Canada

Abstract

Gene-editing techniques such as RNA-guided endonuclease systems are becoming increasingly popular for phenotypic screening. Such screens are normally conducted in arrayed or pooled formats. There has been considerable interest in recent years to find new technological methods for conducting these gene-editing assays. We report here the first digital microfluidic method that can automate arrayed gene-editing in mammalian cells. Specifically, this method was useful in culturing lung cancer cells for up to six days, as well as implementing automated gene transfection and knockout procedures. In addition, a standardized imaging pipeline to analyse fluorescently labelled cells was also designed and implemented during these procedures. A gene editing assay for interrogating the MAPK/ERK pathway was performed to show the utility of our platform and to determine the effects of knocking out the *RAF1* gene in lung cancer cells. In addition to gene knockout, we also treated the cells with an inhibitor, Sorafenib Tosylate, to determine the effects of enzymatic inhibition. The combination of enzymatic inhibition and guide targeting on device resulted in lower drug concentrations for achieving half-inhibitory effects (IC_{50}) compared to cells treated only with the inhibitor, confirming that lung cancer cells are being successfully edited on the device. We propose that this system will be useful for other types of gene-editing assays and applications related to personalized medicine.

Sinha, H., Quach, A.B.V., Vo, P.Q.N. & Shih, S.C.C. ***An automated microfluidic gene-editing platform for deciphering cancer genes.*** *Lab on a Chip 18, 2300-2312 (2018).*

One Cell, One Drop, One Click: Hybrid Microfluidics for Mammalian Single Cell Isolation

Kenza Samlali[1,2], Fatemeh Ahmadi[1,2], **Angela B. V. Quach[2,3]**, Guy Soffer[1,2], Steve C. C. Shih[1-3]

[1]Department of Electrical and Computer Engineering, Concordia University, Montréal, Québec, Canada
[2]Centre for Applied Synthetic Biology, Concordia University, Montréal, Québec, Canada
[3] Department of Biology, Concordia University, Montréal, Québec, Canada

Abstract

Generating a stable knockout cell line is a complex process that can take several months to complete. In this work, a microfluidic method that is capable of isolating single cells in droplets, selecting successful edited clones, and expansion of these isoclones is introduced. Using a hybrid microfluidics method, droplets in channels can be individually addressed using a co-planar electrode system. In the hybrid microfluidics device, it is shown that single cells can be trapped and subsequently encapsulate them on demand into pL-sized droplets. Furthermore, droplets containing single cells are either released, kept in the traps, or merged with other droplets by the application of an electric potential to the electrodes that is actuated through an in-house user interface. This high precision control is used to successfully sort and recover single isoclones to establish monoclonal cell lines, which is demonstrated with a heterozygous NCI-H1299 lung squamous cell population resulting from loss-of-function eGFP and RAF1 gene knockout transfections.

Samlali, K., Ahmadi, F., Quach, A. B. V., Soffer, G., & Shih, S. C. C. ***One Cell, One Drop, One Click: Hybrid Microfluidics for Mammalian Single Cell Isolation****. Small, 2002400 (2020).*

Is Microfluidics the "Assembly Line" for CRISPR-Cas9 Gene-Editing?

Fatemeh Ahmadi[1,2*], Angela B. V. Quach[2,3*], Steve C. C. Shih[1-3]

[1]Department of Electrical and Computer Engineering, Concordia University, Montréal, Québec, Canada
[2]Centre for Applied Synthetic Biology, Concordia University, Montréal, Québec, Canada
[3] Department of Biology, Concordia University, Montréal, Québec, Canada

Abstract

Acclaimed as one of the biggest scientific breakthroughs, the technology of CRISPR has brought significant improvement in the biotechnological spectrum—from editing genetic defects in diseases for gene therapy to modifying organisms for the production of biofuels. Since its inception, the CRISPR-Cas9 system has become easier and more versatile to use. Many variants have been found, giving the CRISPR toolkit a great range that includes the activation and repression of genes aside from the previously known knockout and knockin of genes. Here, in this Perspective, we describe efforts on automating the gene-editing workflow, with particular emphasis given on the use of microfluidic technology. We discuss how automation can address the limitations of gene-editing and how the marriage between microfluidics and gene-editing will expand the application space of CRISPR.

Quach, A. B. V., Ahmadi, F. & Shih, S. C. C. ***Is Microfluidics the "Assembly Line" for CRISPR-Cas9 Gene-Editing?****. Biomicrofluidics 14, 061301 (2020).*

Articles in Preparation for Submission

Viral generation, packaging, and transduction on a digital microfluidics platform

Angela B.V. Quach[1,2], Samuel R. Little[2,3], Steve C.C. Shih[1-3]*

[1]Centre for Applied Synthetic Biology, Concordia University, Montréal, Québec, Canada

[2]Department of Electrical and Computer Engineering, Concordia University, Montréal, Québec, Canada

[3]Department of Biology, Concordia University, Montréal, Québec, Canada

*Corresponding author

Tel: +1(514)-848-2424 x7579

Email: steve.shih@concordia.ca

Chapter 1. Introduction

In this section, we will introduce a short review on topics involving genome engineering technique CRISPR-Cas9 and gene regulation mechanism RNA interference.

1.1 Gene editing and gene regulation

Genome engineering is traditionally performed by the delivery of exogenous genes into the cells with the hope that the cell will integrate the genes into its genome. With recent advances in gene-editing technologies, genome engineering is being revolutionized by the powerful CRISPR-Cas9 system replacing the first gene-editing tools such as zinc finger nucleases[1] and transcription activator-like effectors (TALENs)[2]. This RNA-guided Cas9 system is derived from the adaptive immune system of bacteria and is now being used in almost all laboratories to genetically modify the genome in mammalian cells. CRISPR-Cas9 is short for clustered regularly interspaced short palindromic repeats and CRISPR-associated protein 9 enables a site-specific double-stranded break at the target site that is followed by two natural DNA repair mechanisms of the cell: (1) non-homologous end joining (NHEJ), or via (2) homology directed repair (HDR) when a template DNA fragment is available (**Figure 1.1a**). Both pathways allow for the cell to repair the breaks that can lead to permanent deletions, modifications, or insertions. Although NHEJ repair pathways are more efficient (and hence more frequent) in the cell, there are several new mechanisms that can improve HDR efficiency.[3] Regardless of the efficiency, the multi-functional capabilities of CRISPR are enabling scientists to perform unimaginable experiments that would have been impossible a few years ago – e.g., engineering living organisms with broad applications in the bioindustrial space ranging from treating inherited diseases to solving the bioenergy crisis by modifying agricultural gene crops for

accelerated crop improvement - CRISPR has reshaped the ability to edit DNA in living cells.[4]

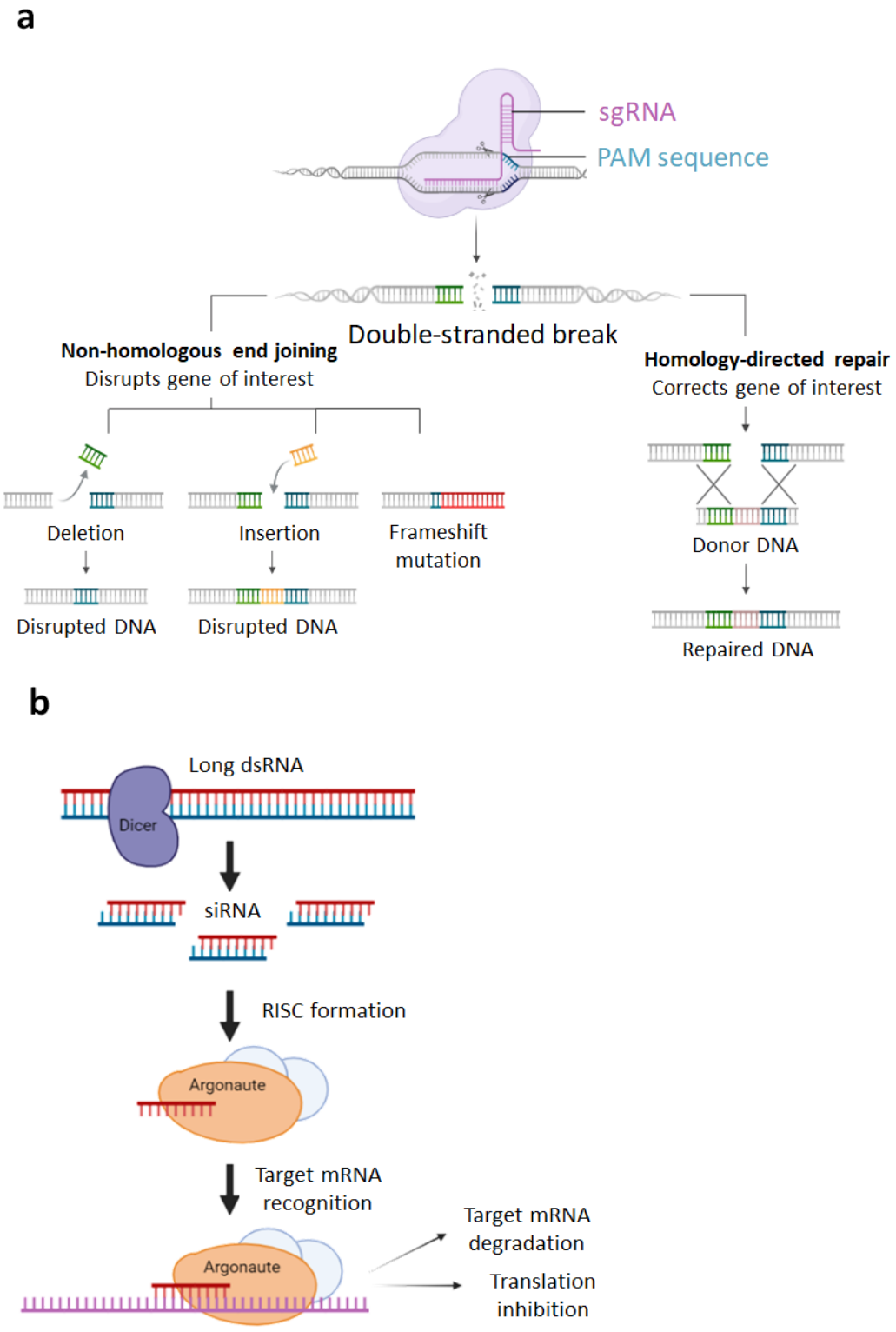

Figure 1.1 – CRISPR-Cas9 and RNAi mechanisms.

Picture (a) reprinted and modified from "CRISPR/Cas9 Gene Editing", by BioRender. Picture (b) produced with BioRender.

Since the discovery of Cas9, gene-editing using CRISPR is rapidly becoming more versatile and easier to use.[5] Recently, there are many other endonucleases orthologues (Cas 12 and Cas 13a) that have been discovered for a variety of applications such as class II Cas12a, Cas13 and class I Cascade. Type V Cas12a contrasts from Cas9 by creating staggered cuts with a 5' overhang at the DNA target site, thereby allowing for integration of orientation specific DNA sequences, which promotes HDR instead of NHEJ.[6] The other recently discovered type VI endonuclease is Cas13a which cleaves ssRNA.[7] As a result, Cas13a has been programmed to cleave target areas on mRNA in bacterial and eukaryotic cells[8]. Lastly, type I Cascade is a complex of multiple proteins that targets DNA and recruits the endonuclease Cas3. Cas3 creates single-stranded nicks as well as degrades the target DNA through its additional exonuclease function. Due to its commonality in nature, researchers are still looking into harnessing the exonuclease activity of Cas 3 for novel applications with mammalian cells.[9]

Primarily known for its purpose to knock out or knock in genes, CRISPR is being redefined for genome regulation functions like CRISPR interference (CRISPRi) and CRISPR activation (CRISPRa).[7, 10] Targeted gene silencing or activation is achieved by using a nuclease-deficient Cas9 (or dCas9) to prevent double stranded breaks while accurately binding to the target DNA with a synthetic guide RNA (sgRNA) and helping to recruit transcriptional factors for the desired regulation.[10b] Aside from its functions, CRISPR is affecting the whole biotechnological spectrum -leading industrial and academic genetic efforts to discover genetic defects in diseases to create new therapeutics [11] to modifying organisms or cellular pathways to fulfill the biofuel's promise [12].

With the advent of CRISPR technology, the field of functional genomics has also taken a huge step forward. Traditionally, loss-of-function screens in mammalian systems were done using RNA interference (RNAi)[13]. Utilized for its gene silencing mechanism, RNAi is an important tool for gene-specific therapeutics involving mRNA targets of disease-associated genes (and drug discovery)[14]. RNAi allows for the inhibition of a target gene's expression through degradation of its mRNA in a sequence-specific manner (**Figure 1.1b**). Concretely, RNAi happens via two different manners where each contrast with the precursors utilized for downstream processing. The first one involves the cleavage of exogenous short hairpin RNA (shRNA) or exogenous double-stranded RNA (dsRNA), into small interfering RNA (siRNAs) by the endoribonuclease Dicer. Then, the siRNA binds to the Argonaute protein where one strand remains bound which becomes the guide strand, while the other is degraded. Thus, this complex along with other proteins called the RNA-induced silencing complex (RISC), is directed to bind to the target mRNA sequence complementary to the guide strand. Upon binding, Argonaute will catalyze the cleavage of the mRNA sequence which will then be degraded.[15] The second approach implicates the handling of micro RNAs (miRNAs) that are derived endogenously from the nucleus and which were initially microprocessed by the microprocessor complex consisting of Drosha bound to DGCR8. A key feature differentiating miRNA from siRNA is that miRNA comprises mismatch bases whereas siRNA has exact base-pairing. Hence, once exported to the cytoplasm, miRNAs go through the same treatment as siRNAs until binding of guide strand to the mRNA sequence. Due to the bases not being perfectly complementary, this will instead drive translation repression as the RISC complex will remain bound to the mRNA transcript. [16]

The mechanism of RNAi mainly serves as a way for cells to regulate gene expression but as seen with CRISPR-Cas9, can also provide a measure of resistance against pathogen or viral infections[17]. Both methods rely on sequence specificity for a nuclease to proceed with enzymatic cleavage. However, both do encounter off-target effects where through optimization of the design (sgRNAs for CRISPR, shRNAs/siRNAs for RNAi) would contribute to a reduced level of off-target effects. Overall, based on a comparative study[18] CRISPR has less off-target effects than RNAi does.

RNAi benefits from using an endogenous machinery in the eukaryotic cell which grants easier execution as only siRNAs or miRNAs have to be delivered into the cell while CRISPR-Cas9 requires for its components (Cas9 and sgRNAs) to be delivered into the cell. The primary difference between these two methods is that RNAi permits gene knockdown at the mRNA level that can be reversible and CRISPR-Cas9 enables permanent gene knockout at the DNA level.[19] Deciding on which to use would depend on the target genes in question behind a study, as complete knockout of lethal genes would be detrimental to the cell whereas an incomplete knockdown of these lethal genes would allow for essential information to be conveyed via observation of decreasing transcript or protein levels.

By using reverse genetics, the causality between genetic abnormalities and their function in a disease is being studied to advance cancer research. Thus far, CRISPR and RNAi have been ultimately used for many large-scale genome screenings in mammalian cancer models [20] as these techniques are useful in revealing genotype to phenotype functions**.** Both techniques are easily adaptable for high-throughput screens either through a pooled or an arrayed fashion (**Figure 1.2**). The pooled format consists of combining the sh/sgRNAs that are delivered in a single population of cells allowing for several

perturbations to be done at once. A following analysis of the cells is then assessed to look at the genes that have been knocked down/out or at the phenotypes being affected from the screen. Due to the presence of a mixed population of cells, pooled screens usually must go through a drug selection stage or undergo fluorescent-activated cell sorting or be subjected to simplistic phenotypic readout such as cell proliferation and cell death[13]. In comparison, the arrayed format permits a single perturbation per different well population of cells, granting an easier genotype to phenotype correlation which can allow for more complex phenotypic interrogations[21]. However, arrayed screens are consequently more expensive and labor intensive, requiring automated liquid-handling machinery to facilitate operations of transferring individual sh/sgRNA libraries to the cells. Thus, an automated and integrated platform that will culture cells for days, enable efficient handling of lentiviruses and reagents, express the gene perturbation machinery targeting an individual gene in target cells, and assay cell phenotypes will be beneficial for these arrayed type experiments to save overall costs and to improve the overall timeframe of the workflow.

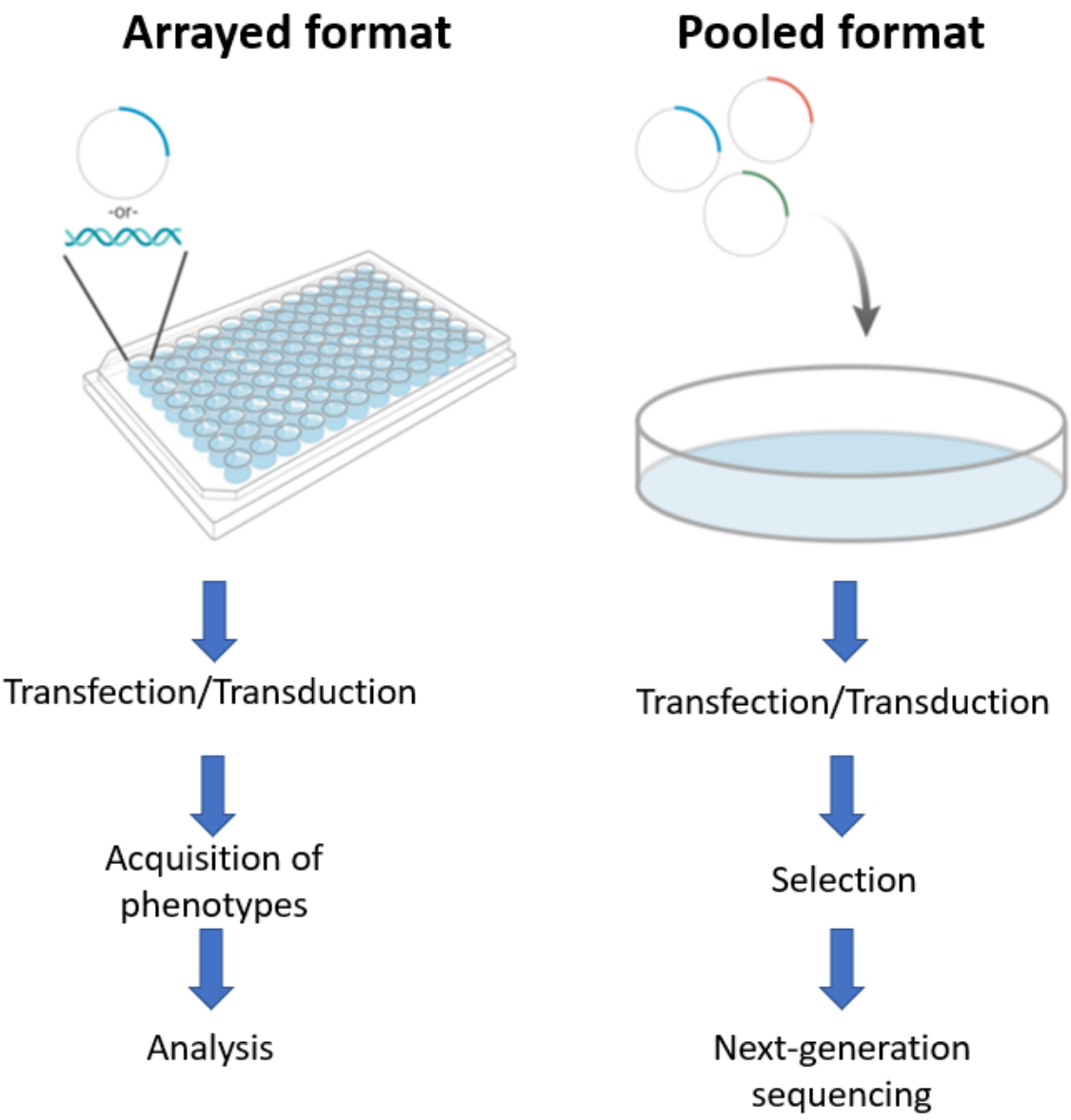

Figure 1.2 – Arrayed screening versus pooled screening.
A single perturbation is applied to the arrayed screening whereas a pool of perturbations is used for the pooled screening. A downstream process is done for the assessment of the screening results.

1.2 Challenges with viral generation, packaging, and transduction

As mentioned above, the steps to perform an effective gene knockout or knockdown in functional genomics are very time consuming, manually intensive, and laborious. The physical workflow of these type of projects consists of four steps: (1) to design and prepare the sh/sgRNA library, usually packaged in lentiviral particles, (2) to deliver the gene disruption machinery to the cell, (3) to analyze the results, and (4) to validate the gene perturbation – all of which can take at least two months to perform (without taking into account the attempts needed for a successful perturbation (**Figure 1.3**))[4a, 10b, 22]. Generally with this workflow, manual handling of these four steps is extremely inefficient due to the constant pipetting and the transferring of cells and reagents to multiple platforms which all can be bypassed if there is access substantial liquid handling machinery. Thus, a key limitation in this aspect is the availability of these costly infrastructures that are well outside of the budgetary reach of many laboratories even though biofoundries are becoming more readily available [23].

There are several ways of delivering the sh/sgRNAs into mammalian cells[24], but the majority of studies[5e, 20a, 20c, 25] heavily rely on lentiviral transduction (**Figure 1.3**). This is mainly due to several advantages they confer, namely their capacity to stably express a transgene surrounded by long terminal repeats (LTR) which promotes integration into the host's genome, the capability to both infect dividing and non-dividing cells and also, they have a wide tropism over a range of species and cell types [26]. As lentiviruses are derived from the human immunodeficiency virus (HIV), they have been engineered over the years to be safer to use by removing virulence factors that would otherwise render them replication-competent and by separating essential viral packaging genes into different

vectors [27]. Furthermore, the lentiviral plasmid containing the transgene is modified to allow the virus to become self-inactivating after integration[28]. Nonetheless, lentiviral particles do come with their challenges – despite all these modifications to make lentiviruses safer to use, there is risk that they can unintentionally restore their replication competency through recombination and thus their pathogenicity is not completely eliminated[26d]. Another safety concern with the use of lentiviruses is the potentiality for oncogenesis. Oncogenesis could occur through two ways where the first one being that random transgene integration into the host's genome can cause insertional mutagenesis. The second way is derived from working with oncogenic transgenes or using libraries of sh/sgRNAs that target tumor suppressor genes. As such, oncogenic modifications that happen in the cells will be carried on by its progeny. Finally, another downside to working with lentiviral particles (and thus, the gene perturbation workflow) is the amount of time and labor required for their production. Lentiviruses have to be packaged in producer cells, harvested, ultra-centrifuged and then titrated in order to know the concentration of the viral titer formed[29]. Current practices of lentiviral production require high concentration of lentiviruses to reduce infection volumes to target cells, but the conventional cell culture platforms do not allow for further reduction of these infection volumes. Thus, several days of lentiviral harvests within large batches of culture and rounds of ultracentrifugation are necessary to achieve a desirable concentration[30]. With copious manual manipulations, one can expose themselves greatly to the biosafety risks involved with handling lentiviruses. Currently, the only solution to mitigate the mentioned potential risks is to have good laboratory practices such as avoiding working with glass shards when handling lentiviruses and to wear appropriate personal protective equipment.

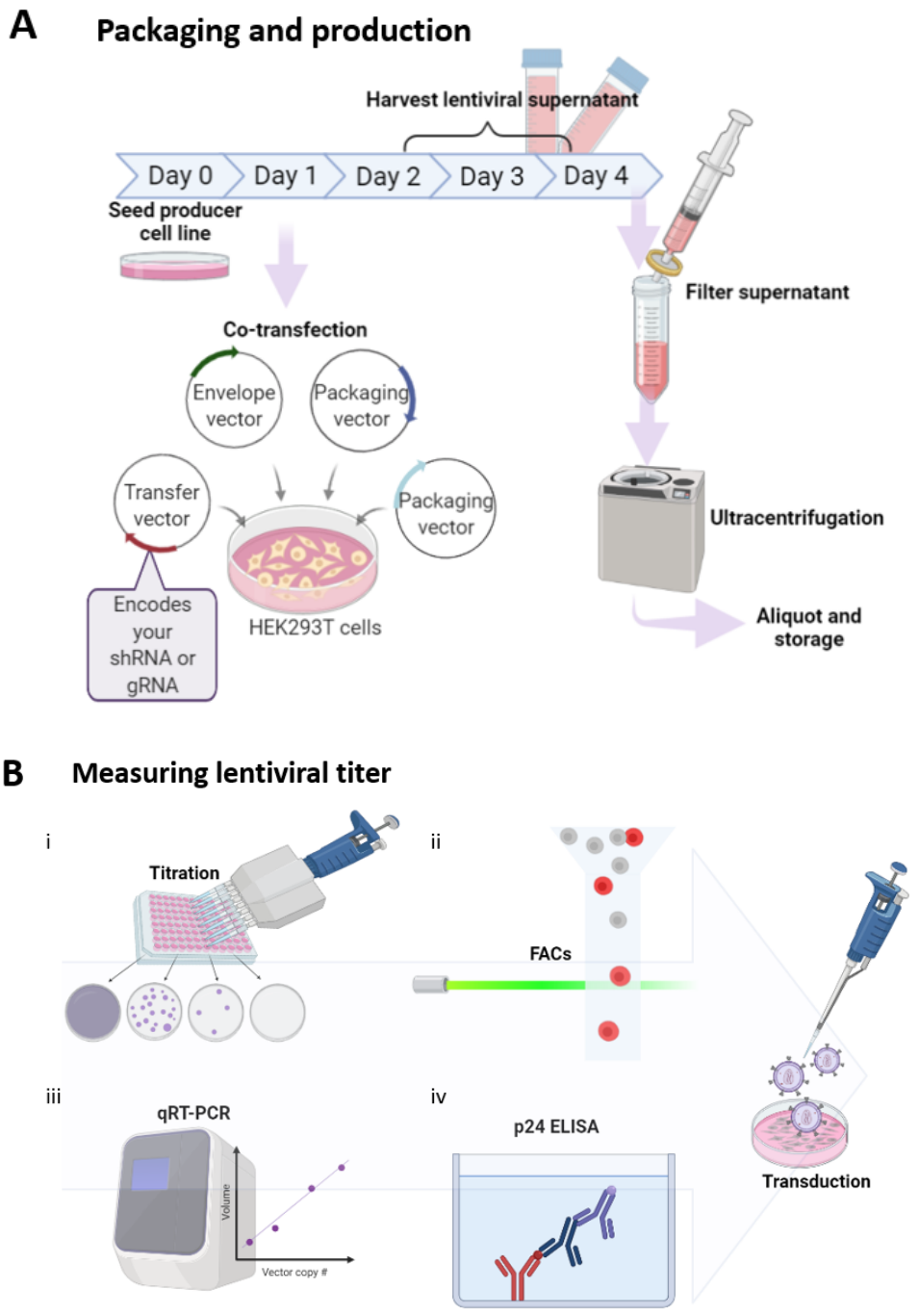

Figure 1.3 – Full process of lentiviral generation (production, titration and transduction). *(a) Workflow for the production and harvesting of lentiviruses: co-transfection is done in a producer cell line where lentiviruses will be harvested in the supernatant over the course of a few days. Overall harvest is then filtered and ultracentrifugated for high lentiviral titer concentration and lentiviruses are aliquoted into small volumes and stored at -80°C. (b) Measuring lentiviral titer: concentration of lentiviruses can be determined through several methods: i) Plaque assays via titration, ii) FACs, iii) qRT-PCR and iv) ELISA targeting the p24 antigen located in the virus' capsid.*

Thus, all these requirements involved for lentiviral production and transduction display the need for improvement in this "state-of-the-art" procedure. Having a standardized gene perturbation platform that can automate the production and transduction of lentiviruses into target cells would improve the workflow. One solution that can provide a "hands-off" workflow for gene perturbation is microfluidics. This technology is modular, enabling easy integration with automation capabilities for *in vitro* cell culture, reagent delivery and fluorescence analysis on device[31]. The low-volume and inexpensive "lab-on-a-chip" aspect give the opportunity to culminate different operations (packaging, delivering, analyzing, and validating) in an all-in-one device to provide convenience in achieving an on-demand lentivirus production with further subsequent gene perturbation and eliminate many of the safety concerns that accompanies the handling and the manipulation of viruses in the macroscale.

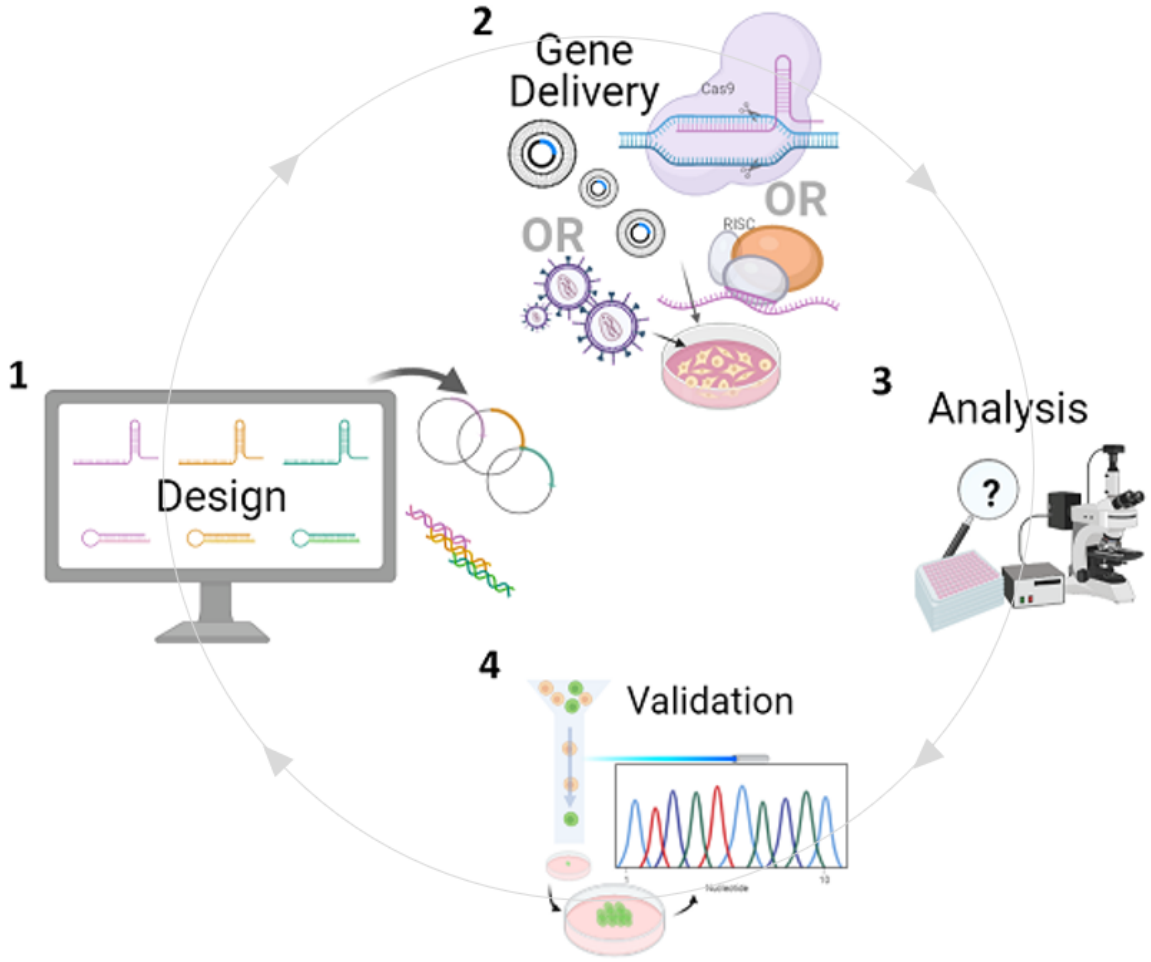

Figure 1.4 – Gene disruption workflow.
1) Design of oligos (sgRNAs or siRNAs) that will target the gene of interest. 2) Nucleic acid delivery to target cells via different gene delivery methods (i.e. liposome-mediated transfection or viral transduction) for the chosen gene disruption technique to be performed. 3) Analysis of the perturbation 4) Validation of the perturbation and when required, selection and expansion of the modified cell line.

1.3 Paradigms of microfluidics

Microfluidics is a relatively modern technology that emerged in the 1950s through the concept of inkjet printers. Over time, increased interest in the miniaturization of systems lead to crucial advancements in the realm of microfluidics. This field is considered as a product created through the influence of molecular biology, molecular analysis[32], microelectronics[33] and biodefence[34]. New methods of fabrication and components/materials throughout the expansion of microfluidics contributed to the development of the current state of the art: 'lab-on-a-chip'. With the ability to manipulate small amounts of fluids at the scale of microliter to attoliter (10^{-6} to 10^{-18}) thanks to the use of microchannels or electrodes, these lab-on-a-chips perform at the miniaturized scale several experiments that are often done in the laboratory. Microfluidics offer a wide range of advantages which include the reduce in cost and volume of samples and reagents, executions of detection and analysis are achieved with high resolution and sensitivity while having possible shorter analysis times and finally, a small footprint associated to devices.

There are different types of microfluidics: 1) channel microfluidics, 2) droplet-in-channel microfluidics, and 3) digital microfluidics (**Figure 1.5**).

Channel microfluidics is characterized by micron-sized dimension (width and height) channels for liquid transport that is driven by external pressure delivered by syringe pumps. With specific viscosity and velocity parameters of the fluid comprised within the geometry of the channel, laminar flow can be experienced when viscous forces are dominant. This allows for the liquid flow to be streamlined which would permit several streams of reagents to flow along with each other in the same channel without mixing. However, when the viscous forces are irrelevant, turbulent flow will occur which can

allow for mixing[35]. The laminar flow property is one of the advantages in using microfluidic devices since molecules can be controlled more precisely leading to the formation of static and dynamic gradients which are needed in many biological applications.[36] For example, organs can be cultured on a chip where medium transport is needed to renew nutrients for the cells but also to evacuate waste[37]. Another case illustrates sample extraction and purification followed by target molecule detection when combined with an electric field for diagnostic applications[38]. The use of channel microfluidics is widespread, but some complexities such as needing several syringe pumps for different reagents, convoluted fabrication techniques for special features (i.e. creating mixing chambers) and integration of microvalves for fluid motion control may compel users to exploit other types of microfluidics.

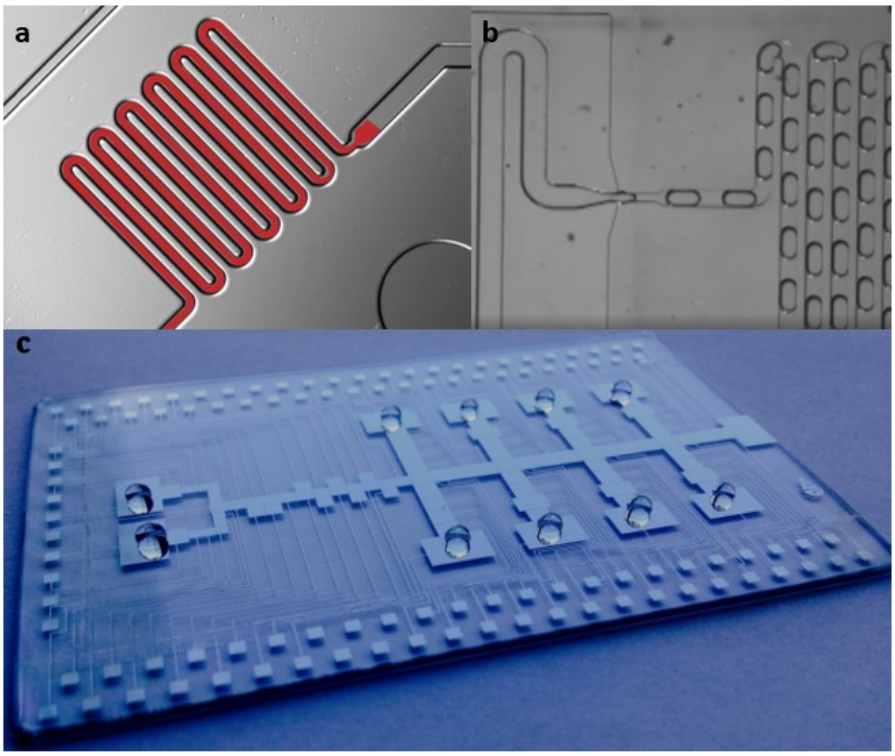

Figure 1.5 – Microfluidic paradigms. *(a) Microchannels. Reproduced with permission from Dr. Samuel Sia's laboratory. (b) Droplets-in-channel. Reproduced with permission from the Royal Society of Chemistry.[39] (c) Digital microfluidics.*

Droplet-in-channel microfluidics is best known for its high-throughput benefits as this platform can generate thousands of discrete droplets via multiphase immiscible flow in microchannels. A few techniques developed for droplet generation are done by changing the microchannel geometry for shearing of fluids and precise flow control for droplet generation can be achieved with a syringe pump system or compressed-air-driven microfluidic system [40]. Thus, its desirable high-throughput aspect allows for several different assays in a wide scope of applications that can be carried out on this platform. For example, droplet formation is very popular for single-cell analysis where microorganisms can be encapsulated in droplets that subsequently act as a micro-bioreactor[41]. Co-encapsulation or merging with other substrates such as enzymes[42], detection probes[43], nanoparticle-filled drugs[44], etc., offer a myriad of studies with several downstream manipulations like incubation times, detection, and sorting. Nonetheless, as with channel microfluidics, the need for a flow control system (i.e. syringe pumps) can contribute to excessive complicatedness in setting up the entire framework. Furthermore, there is a difficulty to address each droplet individually in a droplet microfluidic device unless it has been fabricated to hybridize with digital microfluidics to give it precise control over individual droplets[39, 45].

Finally, digital microfluidics (DMF) consists of manipulating picoliter to microliter volume-sized droplets on an array of electrodes which is the central paradigm used for this research project. The driving force behind the movement of droplets across electrodes are electrostatic forces, analogous to an electrically charged comb that can bend a stream of water towards the comb. Thus, by applying an electric potential difference (also known as voltage), a change in the contact angle between the droplet and an actuated electrode will

occur, leading to an increased area of contact between the droplet and the electrode (**Figure 1.6)**. This phenomenon is termed as 'electrowetting' which was first observed by Gabriel Lippmann back in 1875. Eventually, the idea of using a thin insulating layer, also known as a dielectric, to separate the conductive liquid from the electrode was introduced to avoid the problem of electrolysis (burning/breakdown of the electrode).[46] The concept was then modernized to be described as 'electrowetting on dielectric (EWOD)' and is the underlying core mechanism of digital microfluidics.

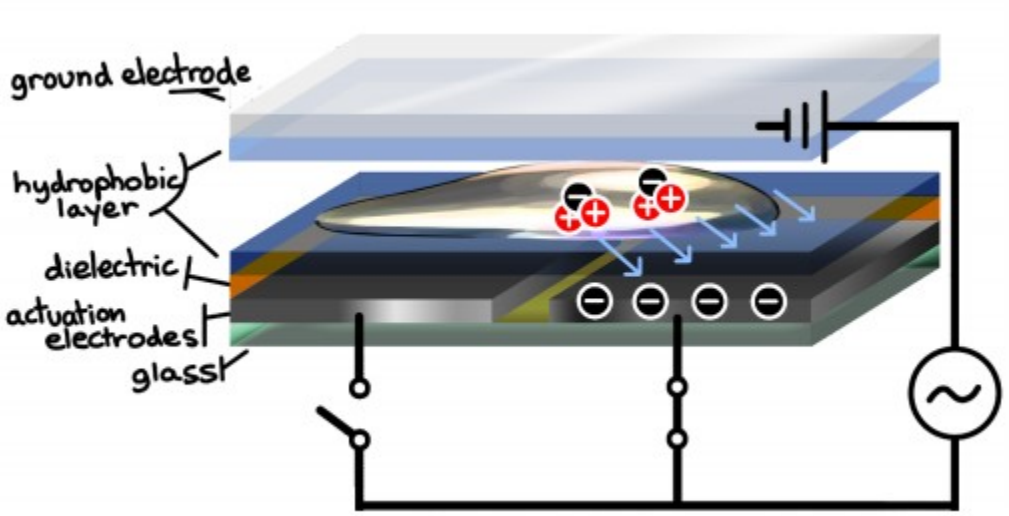

Figure 1.6 – Droplet movement driven by electrostatic forces on actuated electrode.

The DMF device can be composed of single-plate or two-plate configuration in which the latter format is used for this research project. The top plate is made from a glass plate coated with a conductive transparent metal called indium tin oxide (ITO), along with a hydrophobic layer and is used as a continuous grounding electrode for the circuit. The bottom plate is generally made of a glass substrate patterned with chromium electrodes which is coated with a thin insulating dielectric and a hydrophobic layer to limit the surface tension of a droplet to substrate (**Figure 1.7**). Two-plate devices mostly operate droplets

in air but sometimes an oil-filled medium is put in place to decrease the voltage required for droplet movement and/or to reduce the evaporation rate of a droplet[47]. Thus, droplet movement in a two-plate format will not only experience driving electrostatic forces but also experience a shear force from between the plates and the droplet and a viscous drag force caused by the filler medium[48]. Comparatively to the single-plate format which only is capable of having droplets mixed and merged, the two-plate configuration additionally allows the operations of dispensing droplets from reservoirs and splitting droplets.

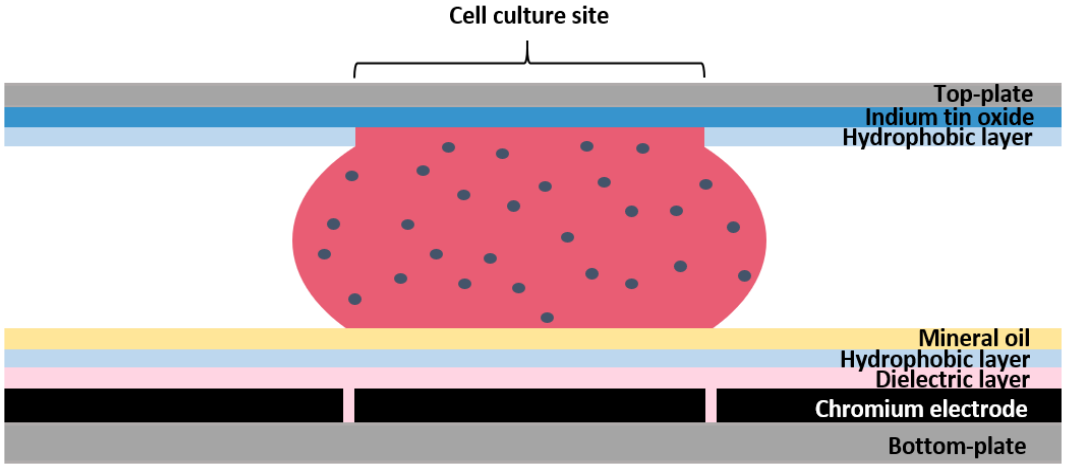

Figure 1.7 – Side-view schematic of two-plate configuration for DMF with culture site.

Hence, a principal advantage that DMF has among the other paradigms of microfluidics is the individual addressability it has on a droplet as those in droplet microfluidics are controlled in series. Moreover, there is no cross-contamination between droplets of different reagents or samples as Pluronics, an amphiphilic polymer, are added to create micelles surrounding the droplet [49]. Thanks to the 'm x n' array geometry of electrodes on DMF, it is relatively straightforward to reconfigure the design to a user's

preference according to the types and amounts of droplet operations needed in their application. Lastly, DMF can also be easily integrable with software-friendly automation systems[50], thus granting droplet operation to be automated and minimizing the manual intervention needed from a user.

A main disadvantage when working with DMF is the device longevity, especially when it comes to working with high protein content solutions. This is due to the adsorption of the proteins to the hydrophobic surface which in the long run, will cause the surface to become 'stickier' and reduce droplet movement, a term called 'biofouling'. Several solutions have been implemented to overcome this challenge whereas mentioned above, the practice of adding Pluronic additives has helped with decreasing the effect of biofouling. This is due to their micelle formation which has been shown to favor the encapsulation of biomolecules within the droplet, limiting the interaction between these biomolecules and the device's surface [49]. Another solution is to use an immiscible oil which isolates the droplets from the hydrophobic surfaces, allowing adsorption to be reduced[51]. Researchers have also worked on developing thin replaceable films or lubricant infused porous films that would allow the reuse of a device thereby alleviating the issues of biofouling[52].

Integrating DMF with cell-based applications has become very prominent as it reduces costs and volume of expensive reagents, allows for precise control of droplets, and has easy design reconfiguration for specific assays. With continuous improvement for reducing biofouling, researchers have been able to bring cells for culture upon the device. Initial progress of cell culture on device has started with suspension cells where a group was able to show movement of droplets containing human fetal osteoblast cells without

any adverse effect on the cell viability[53]. Barbulovic-Nad et al.[54] then commenced the first cell-based assay on DMF by conducting a cytotoxicity assay using Jurkat cells and then measuring their viability on device. They demonstrated that there was no significant difference in cell viability and proliferation upon electrode actuation and that the cytotoxic assay was able to outperform an identical assay in the well-plate format. Eventually, adherent cell lines were used for culture on DMF by culturing them over extracellular matrix spots on the ITO plate[55]. As a result of this, the term 'passive dispensing' has been applied to interpret the passing of a cell medium droplet over a culture site, thereby removing the old medium and replacing it with fresh medium. This favored the renewal of medium to cell without any concern of cell drying or cell death. However, due to irregularity of these spots preventing further reproducibility in their design, it has led to the implementation of a specialized technique called 'Teflon lift-off'[56]. Teflon lift-off is a straightforward procedure that provides patterned hydrophilic spots on the ITO top-plate. These hydrophilic spots can then be used to seed and culture adherent cells on in a reproducible manner.

Ultimately, more complex experiments were done on DMF in which we have previously reported automating gene-editing using digital microfluidics to decipher cancer pathways[31a]. The premise was to automate lipid-mediated transfection to deliver plasmid-based CRISPR-Cas9 machinery into a small lung carcinoma cell line for knockout of a stably expressing reporter gene within the cells as a proof-of-principle. Then target of an oncogene in the same cell line was done using an image-based analysis technique to analyze edited cells. Thus, this has set the foundation of this project in which the objectives will be discussed in Chapter 1.5.

1.4 Special focus on microfluidic devices for lentiviral transduction

Since the development of gene-editing, a lot of emphasis has been given for gene delivery on microfluidics. However, most of them focuses on chemical transfection such as liposome-mediated transfection and mechanoporation or electroporation[57]. Little attention has been given to gene delivery using lentiviral transduction on microfluidics, most probably due to biosafety issues ensued from its manipulation. Currently, a group from the Georgia Institute of Technology and Emory University has been working on harnessing lentiviral transduction on microfluidics to enhance its efficiency. Tran et al.[58] have demonstrated that microfluidics transduction allows for a significant higher surface area and volume ratio between cells and lentiviruses, bringing both parties into closer proximity. This permits for a higher concentration of lentiviruses without needing to increase the quantity of lentiviruses (**Figure 1.8**). By coating their polystyrene device with retronectin to immobilize non-adherent cells, they perfused lentiviruses through the channel at low concentrations to sustain a constant fresh supply of lentiviruses to the cells. In comparison with well plates, they have observed that the kinetics of lentiviral transduction are faster with five hours of incubation on device comparable to 24 hours in a 6-well plate for GFP expression in transduced cells resulting in a >4 fold increase in transduction efficiency with the microchannel. Moreover, they investigated transducing (hemopoietic stem cells) to correct hemophilia A in a murine model. They first transduced Sca-1+ cells (stem cells antigen-1) collected from mice using highly concentrated and clinically processed lentiviruses that encoded for the fVIII factor, (a substance needed for the body to form blood clots) on microfluidics. Then, they transplanted the transduced cells into lethally irradiated fVIII-deficient mice and monitored the plasma fVIII levels in the

recipients every 2 weeks for 2 months until the fVIII levels stabilized. The group found that 3 out of 5 mice transplanted with microfluidic-transduced cells had plasma fVIII production levels within the normal range, whereas those that were transplanted with cells transduced in a 6-well plate with the same number of transducing units have mild hemophilia levels. Thus, they were able to illustrate that the usage of lentiviruses on microfluidics exhibited pre-clinical safety and efficacy.[58b]

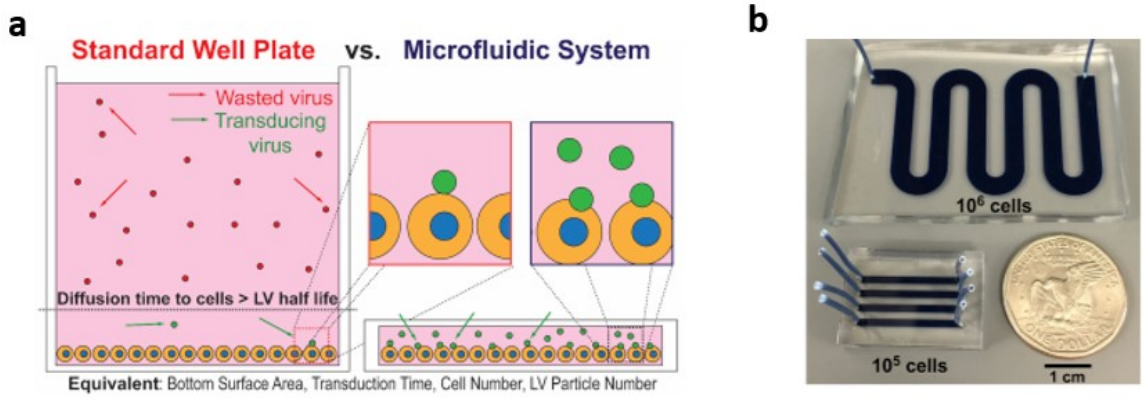

Figure 1.8 – Channel microfluidic device used for lentiviral transduction.
(a) Comparison of viral transduction applied to a well plate versus in a microfluidic channel showing the closer proximity brought upon viral particles towards the target cells. (b) Microfluidic device utilized for viral transduction. Reproduced with permission from American Society of Gene & Cell Therapy.[58b]

Despite the microchannel device's success at obtaining a higher transduction efficiency, in order to reach clinically adequate results, they had to gather a high-titer viral particle in the first place. Thus, this limits the expandability for large-scale clinical settings in gene therapy. Hence, another group from the Biological Microsystems department in Cambridge has developed another microfluidic transduction device (MTD) that colocalizes target cells and lentiviruses together on a semi-permeable membrane to accomplish several-fold increases in transduction efficiency[59]. They achieve this by introducing both cells and viruses through a channel into a chamber where they are pinned against the semi-permeable membrane which 'increases the rate of interaction between' both bodies. After a

period of time, they reverse the fluidic flow acting through the membrane while additional fluid is pushed across the membrane', enabling the recovery of cell and viruses into another channel (**Figure 1.9**). By using this method, they have to determine flow rates that should minimize shear stress for decreasing the risk of cell damage.

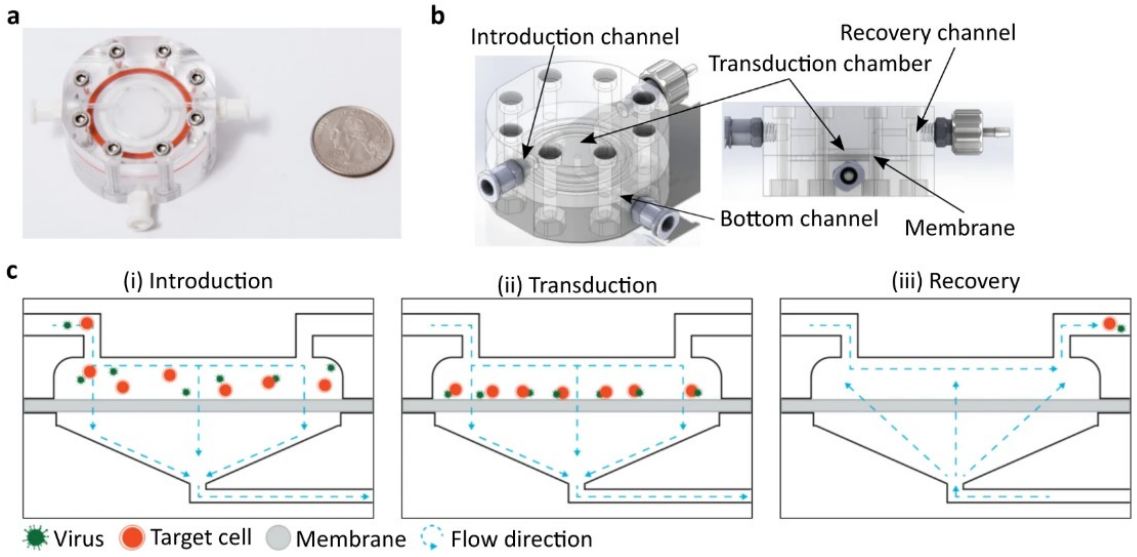

Figure 1.9 – Channel microfluidic device used for enhanced viral transduction.
(a) Microfluidic device utilized for enhanced viral transduction efficiency. (b) Microfluidic design showing the chamber intended for viral transduction of target cells and the introduction and recovery channel for the lentiviral particles and cells. (c) Schematic of the process performed for the i) introduction of lentiviral particles and target cells, ii) the colocalization of both parties onto a semi-permeable membrane for transduction and iii) the retrieval of the transduced cells and lentiviruses by reversing the flow direction. Reproduced with permission from Scientific Reports.[59]

These approaches have been used to reduce volumes for transduction, to enable faster transduction rate, and to overcome limitations with costs and scalability. While these represent important steps forward, the methods do not integrate lentiviral packaging and production, as they are limited in the complexities of cell cultivation of a packaging cell line, transfection of the plasmids, media and reagent exchange, and harvesting the viral particles. Furthermore, these studies also rely on external syringe pumps which are more difficult to integrate automation into the process and to perform multiplexed analysis.

1.5 Thesis objectives

To address the challenges described above, we introduce the first automated technique to package, prepare, and transduce lentiviruses. We call it LENGEN for LENtiviral GENeration (representing steps of in lentiviral production and transduction) on a digital microfluidics platform. In this work, we report the novelty behind the automated platform which can allow: (1) the generation of lentiviral particles on-demand containing gene-editing machinery, (2) the culture, the edit, and the analysis of edited/non-edited cells directly on device and (3) a 'hands-off' gene-editing workflow for safer handling of lentiviruses.

My research objectives are divided into these following steps:

1. Device design: The device layout was created for cell culture of different cell lines in which an area is dedicated for the producer cells to package and produce lentiviral particles for infection of the target cells.
2. Viral characterization of the DMF device: Viral production and viral titer measurement on-chip procedures were optimized by using a simple fluorescent reporter lentiviral vector to first infect an easy-to-transfect cell line. Then, larger lentiviral payload were used to evaluate its effects on a non small cell lung cancer cell line and breast cancer cell lines (MCF-7 and T47DKB-Luc).
3. Proof-of-principle: Packaging, production, and transduction to knockout an endogenous fluorescent marker in a non-small-cell lung cancer cell line (H1299) was done on-chip and off-chip. Genomic cleavage assays were used to validate knockout of the gene.

4. Application: Packaging, production, and transduction to knockout and knockdown the estrogen receptor alpha (ERα or ESR1) in a breast cancer cell lines (MCF-7) was done on-chip and off-chip. To assess ESR1 knockout, genomic cleavage assays were done and RT-qPCR was used to validate ESR1's gene expression.

These results (to our knowledge) are the first of their kind and we hope that this procedure will allow to accelerate (days instead of weeks) lentiviral production and transduction processes which can lessen the labour associated with enhancing lentiviral generation and transduction.

Chapter 2. Methodology

In this chapter, I will describe the methodology for incorporating the process of lentiviral packaging, production, and transduction on digital microfluidics (microscale) and the same procedures for macroscale experiments. Validation methods are described towards the end of this section.

2.1 Reagents and materials

Microfluidic device fabrication reagents and supplies included chromium-coated glass slides with S1811 photoresist from Telic (Valencia, CA), indium tin oxide (ITO)-coated glass slides, RS =15-25Ω (cat no. CG-61IN- S207, Delta Technologies, Loveland CO), MF-321 positive photoresist developer from Rohm and Haas (Marlborough, MA), CR-4 chromium etchant from OM Group (Cleveland, OH), AZ-300T photoresist stripper from AZ Electronic Materials (Somerville, NJ), DuPont AF from DuPont Fluoroproducts (Wilmington, DE). Transparency masks for device fabrication were printed from CAD/Art (Bandon, OR). General chemicals for tissue culture were purchased from Wisent Bio Products (Saint-Bruno, QC, Canada). Invitrogen Lipofectamine 3000 Transfection Reagent was purchased from Thermo Fisher Scientific (Waltham, MA). Unless specified otherwise, general-use chemicals and kits were purchased from Thermo Fisher Scientic and Sigma-Aldrich (St. Louis, MO). Plasmids for this study were purchased from Addgene or donated (**Figure S1**) and primers (**Table 2.1-2.2**) were purchased from Invitrogen (Waltham, MA).

Table 2.1 – CRISPR target sequences

Custom LentiCRISPRv2 plasmids	Custom sequence (nucleotides in gray are Esp3I sticky ends)	PAM	Source
LCV2_eGFP_12	Oligo1:CACCGGGGCGAGGAGCTGTTCACCG Oligo2: AAACCGGTGAACAGCTCCTCGCCCC	GGG	Shalem et al., 2014
LCV2_eGFP_497	Oligo3: ACCGTCAAGATCCGCCACAACATCG Oligo4: AACCGATGTTGTGGCGGATCTTGAC	AGG	Shalem et al., 2014
LCV2_eGFP_683	Oligo5: ACCGCCATGCCGAGAGTGATCCCGG Oligo6: AACCCGGGATCACTCTCGGCATGGC	CGG	Shalem et al., 2014
LCV2_ESR1_76	Oligo7: CACCGCGCCGTGTACAACTACCCCG Oligo8: AAACCGGGGTAGTTGTACACGGCGC	AGG	This study
LCV2_ESR1_91	Oligo9: CACCGCGCGGCGTTGAACTCGTAGG Oligo10: AAACCCTACGAGTTCAACGCCGCGC	CGG	This study
LCV2_ESR1_320	Oligo11: CACCGTACCTGGAGAACGAGCCCAG Oligo12: AAACCTGGGCTCGTTCTCCAGGTAC	CGG	This study

shRNA targeting estrogen receptor alpha (ERα) and a non-target shRNA in pLKO.1 backbone were used:

Non-target shRNA (Custom made by Dr. Mader's lab):
5'- GCGCGATAGCGCTAATAATTT -3'
ERα shRNA 1 (Sigma-Aldrich TRCN0000003300):
5'- CTACAGGCCAAATTCAGATAA -3'

Table 2.2 – Primers used in this study

Primer	Purpose	Sequence (5'–3')
LCV2_eGFP_12_F	Colony PCR	TTTTCTGCTCGCCGCTCAGGAA
LCV2_eGFP_497_F	Colony PCR	TCAAGATCCGCCACAACATCGGTT
LCV2_eGFP_683_F	Colony PCR	ATGCCGAGAGTGATCCCGGGTT
LCV2_ESR1_76_F	Colony PCR	CACCGCGCCGTGTACAACTA
LCV2_ESR1_91_F	Colony PCR	GCGGCGTTGAACTCGTAGGGTT
LCV2_ESR1_320_F	Colony PCR	CACCGTACCTGGAGAACGAGCCCAG
LCV2_cPCR_R	Colony PCR	TGTCCACCACTTCCTCGAAGTTCC
NeoRoverhang_F	Overhang PCR	TTGCATTCTAGACTGAGGCGGAAAGAACCAG
NeoRoverhang_R	Overhang PCR	CACAGCTTCTAGATGACGCTCAGTGGAACGA
LCMN_EcoRI_F	PCR amplification	TTGAATTCTAGACTGAGGCGGAAAG
LCMN_overhang_R	PCR amplification & overhang PCR	ACTGAACGTCTCTTAACGCGTCACTTGTACAGC
LCV2_overhang_F	PCR amplification & overhang PCR	TAGTTAAGAGACGCGTTAAGTCGACAATCAACCTCTG
LCV2_EcoRI_R	PCR amplification	TTCAAGACCTAGCTAGCGAATTCA
LCMNv2_cPCR_R	cPCR	CGCCAAAGTGGATCTCTGCTGTC
hU6_prom_F	Sequencing	GAGGGCCTATTTCCCATGATTC
NeoR_F	Sequencing	GAACAAGATGGATTGCACGC

2.2 Device fabrication and assembly

Digital microfluidic devices were fabricated following methods as introduced previously [31a]. Briefly, designs were drawn using AutoCAD 2018 (Autodesk, San Rafael, CA) and photomasks were then printed in high-resolution (20,000 dpi) by CAD/Art Services Inc (Bandon, OR). The bottom-plates bearing patterned electrodes were formed by standard photolithography techniques. Chromium substrates coated with photoresist were UV-exposed through the photomask (7s, 42.4 mW/cm^2) to imprint the transparency mask designs. Substrates were then developed in MF-321 positive photoresist developer (2

min, shaking), rinsed with DI water, dried under a stream of nitrogen and baked for 1 min at 115°C. The exposed chromium was then etched using CR-4 chromium etchant (3 min) and substrates were then rinsed with distilled water and dried under a stream of nitrogen. Finally, devices were immersed in AZ300T photoresist stripper (3 min) to remove any remaining photoresist before being rinsed and dried under a stream of nitrogen. Once the patterning step was completed, the substrates were immersed in a silane solution consisting of deionized water, isopropanol and 3-(Trimethoxysilyl)propyl-methacrylate (50:50:1) for dielectric priming during 15 min. Substrates were rinsed with isopropanol, distilled water and then dried under a stream of nitrogen. Prior to the addition of the polymer coating to complete the process, thermal tape was added on top of the contact pads to facilitate later removal of the polymer coating from the contact pads and allow electrical contact for droplet actuation. Parylene-C was used as a dielectric which was deposited by chemical vapor deposition in a SCS Labcoter 2 PDS 2010 (Specialty Coating Systems, Indianapolis, IN) achieving a uniform thickness of 7 μm. 1% Teflon-AF 1600 in FC-40 was used as a hydrophobic coating and was spin-coated in a Laurell spin-coater at 1000 rpm for 30 s followed by post-baking on a hot-plate (165°C, 10 min).

The DMF top-plates consist of a continuous ground electrode formed from an indium tin oxide (ITO) coated glass substrate. For typical ground plates, ITOs were spin-coated with the 1% Teflon-AF 1600 using the same program as described in the bottom-plate fabrication procedure. ITOs that have an array of hydrophilic spots (i.e., circular regions of exposed ITO) for on-chip tissue culture were microfabricated using a Teflon-liftoff procedure (following procedures described previously[31a]. ITOs were cleaned by immersion in an RCA solution comprising of distilled water, 28% aqueous ammonium

hydroxide, 30% hydrogen peroxide (5:1:1 v/v/v) for 30 min at 80°C on a hotplate. After rinsing, drying and dehydrating (2 min at 95°C), the substrates were spin-coated with Shipley S1811 photoresist (10 s, 500 rpm, ACL=100 rpm and 60 s, 3000 rpm, ACL=500 rpm) and baked at 95°C for 2 min. Slides were cut to the desired size (i.e.: 50 x 75 mm) using a Cuter's Mate (Creator's Stained Glass, Victoria, BC) and vented under a stream of nitrogen. Substrates were exposed through the photomask with an array of 12, 1 mm diameter circular features and two ~2 mm diameter circular features (10 s, 42.4 mW/cm^2) and were developed in MF-321 (3 min). After rinsing, air-drying and dehydrating (1 min, 95°C), top-plates were then flood exposed (10 sec, 42.4 mW/cm^2), spin-coated with 1% Teflon-AF 1600 (10 s, 500 rpm, ACL = 100 rpm and 60 s, 3000 rpm, ACL = 500), and post-baked on a hotplate (165°C, 10 min). After allowing to cool on aluminum foil for 2 min, substrates were immersed in acetone with gentle agitation for 10-15 s until the Teflon-AF over the patterned sites was lifted off. After being rinsed with DI water and dried under a stream of nitrogen, the substrates were post-baked to reflow the Teflon-AF at 165°C, 210°C and 300°C for 5 min at each temperature.

Complete devices were assembled with the continuous ground ITO top-plate and the chromium electrode-bearing bottom plate, being joined by stacking two layers of double-sided tape to a gap height of approximately 140 μm. Alignment of the ITO top plate above the bottom plate was performed with care such that smaller circular features aligned with the target cell culture regions and the larger circular features aligned with the HEK293T cells culture regions (see **Figure 3.1**).

2.3 Automation setup and device operation

The automation system (**Figure 2.1**) consists of a graphical user interface run by a Python program that is used to control an Arduino Uno microcontroller. A driving potential of 2.5 V_{P-P} or ~500 V total was generated by amplification of a sine wave output from a function generator (Agilent Technologies, Santa Clara, CA) operating at 10 kHz by a PZD-700A amplifier, (Trek Inc., Lockport, NY) and delivered to the PCB control board. The Arduino controls the state of high-voltage relays (AQW216 Panasonic, Digikey, Winnipeg, MB) that are soldered onto the PCB control board. The logic state of an individual solid-state switch is controlled through an I^2C communication protocol by an I/O expander (Maxim 7300, Digikey, Winnipeg, MB). This control board is mated to a pogo pin interface (104 pins), where each switch delivers a high-voltage potential (or ground) signal to a contact pad on the DMF device. See our GitHub registry (https://github.com/shihmicrolab/Automation) to assemble the hardware and to install the open-source software program to execute the automation system.

On-chip experiments were done through reagent loading by pipetting a droplet of liquid onto the outer-edge of a reservoir electrode and adjacent to the gap between the bottom and top plates and actuating the reservoir electrode. This will allow the droplet to slip under the top plate and be 'sandwiched' between the two plates. Once inside the reservoirs, the droplets were then actively dispensed, moved, mixed or merged by sequential actuation of adjacent electrodes on the bottom plates. Active dispensing was achieved over three electrodes and results in a droplet with a diameter of the same size as the electrodes (i.e. a unit droplet). To initiate passive dispensing, it is achieved by moving an actively dispensed droplet over the vacant lift-off hydrophilic spot. At times, contents

on this spot may be displaced with the contents of a new source droplet. Generally, all droplets containing proteins were supplemented with 0.05% Pluronics F-127 (ThermoFisher). Waste and unused fluids were removed by delivering them to waste reservoirs and removed using KimWipes (Kimberly-Clark, Irving, TX).

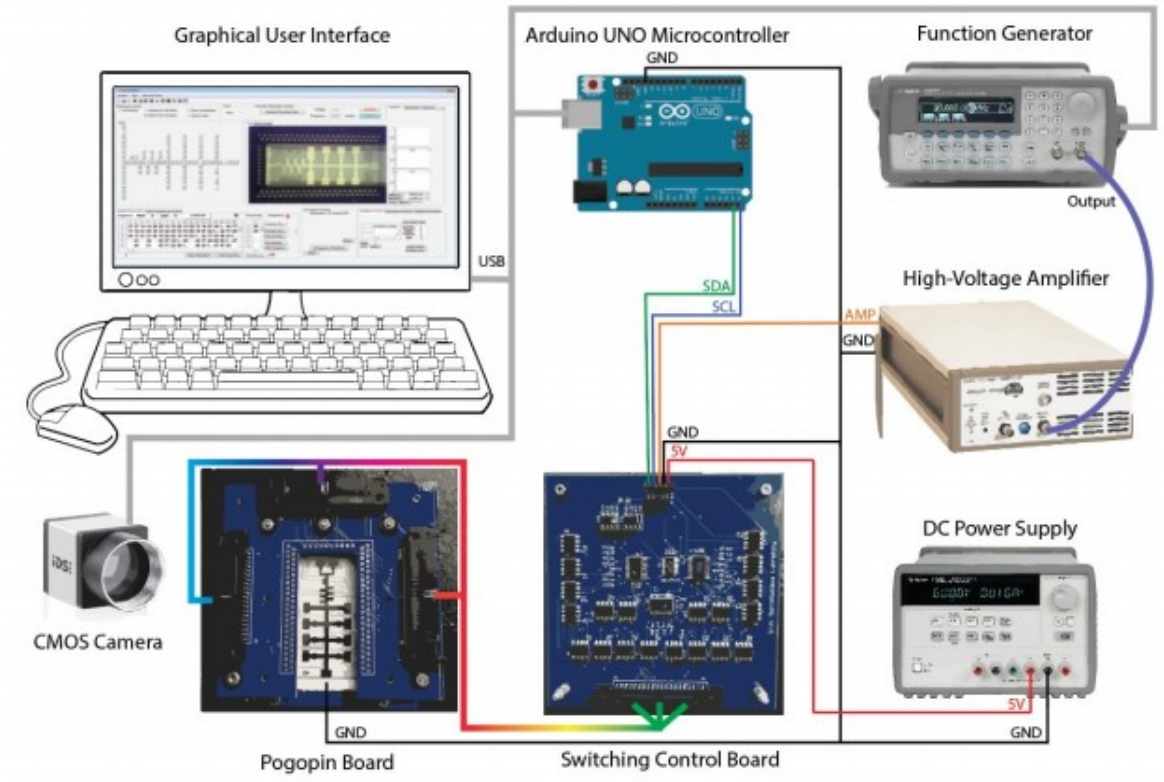

Figure 2.1 – Digital microfluidic automation system for gene-editing

2.4 Lentiviral vector digestion, oligo annealing, and cloning

For lentiviral plasmids, we followed a similar protocol described from the Zhang lab.[5e, 20a] Briefly, 20 bp sgRNA scaffold were synthesized as oligonucleotides (ThermoFisher, Waltham, MA) after being designed via the Benchling online platform. The oligos were designed with Esp3I sticky ends (such that they can be ligated to the lentiCRISPR_v2 backbone (Addgene, plasmid #52961) (see Table 1 for all synthesized

guides with sticky ends). The backbone was first digested using the Esp3I restriction enzyme by following the Thermofisher manufacturer's protocol (Waltham, MA). The digestion reaction consisted of 2 µL Anza^{TM} 10X buffer, 1 µL Anza^{TM} Esp3I enzyme, 2 µL DTT (10mM), 1 µg template DNA and topped to 10 µL final volume using diH_2O. The reaction tube was incubated at 37 °C for 15 min and immediately heat-inactivated at 65 °C for 20 min to avoid star-activity. The digested plasmid was run through a 0.8% agarose gel in TAE buffer at 100 V for 45 min and the backbone band (~13 kb) was gel purified using the GeneJET gel extraction kit (ThermoFisher, Waltham, MA). Each pair of oligos were then phosphorylated and annealed using Anza^{TM} T4 PNK by following the manufacturer's protocol. The phosphorylating and annealing reaction consisted of 1 µL oligo 1 (100 µM), 1 µL oligo 2 (100 µM), 1 µL 10X T4 Anza^{TM} ligation buffer, 0.5 µL Anza^{TM} T4 PNK and 6.5 µL distilled water. Each reaction tube was put in the thermocycler using the following parameters: 37 °C for 30 min, 95 °C for 5 min and then ramping down to 25 °C at 5°C/min. The annealed oligos were then diluted with sterile water at 1:200 dilution. Following the annealing step, the annealed oligos were then ligated with the purified, digested lentiCRISPR_v2 backbone with the New England BioLabs T4 ligase (Whitby, ON) following the manufacturer's protocol. The ligation reaction consisted of 1 µL annealed oligo (gRNA), 50-100 ng backbone vector, 1 µL 10X T4 buffer, 1 µL T4 ligase and topped with nuclease-free water up to a final volume of 10 µL. The reaction tubes were incubated at room temperature for 10 min. The assembled products were transformed by heat-shock procedures (42 °C, 1 min; incubation on ice; 3 min) into a competent Stbl3 *E. coli* strain. The transformed products were grown on LB/ampicillin agar dishes and 3 colonies were picked for colony PCR as quick analysis for insert

confirmation. Each colony that was picked was diluted in 20 µL of diH_2O. For the colony PCR procedure, one reaction consisted of 16.8 µL of Phusion high-fidelity mastermix buffer, 1 µL of forward primer (10 µM), 1 µL of reverse primer (10 µM), 1 µL of the diluted colony and 0.2 µL of the high-fidelity Phusion polymerase (Thermofisher, Waltham, MA). The following PCR thermocycling conditions were used: initial denaturation at 98 °C for 30 s followed by 35 cycles of denaturation at 98 °C for 10 s, annealing at 60 °C for 30 s and extension at 72 °C for 30 s/kb, and a final extension step at 72 °C for 5 min. PCR products were loaded into a 0.8% agarose gel in TAE buffer and resolved at 130 V for 30 min. Positive clones were expected to yield a ~2 kb amplicon and negative clones were expected to yield no amplicons. The positive clones were then grown overnight liquid culture of 5 mL LB before being DNA purified. The constructed plasmids were verified by Sanger sequencing (Eurofins Genomics; Toronto, ON, Canada).

2.5 New plasmid construction

Due to needing a fluorescent marker on the lentiviral backbone for easier visualization on DMF experiments and needing a different mammalian antibiotic marker, pLentiCRISPR_mCherry was purchased (Addgene, plasmid #75161). Overhang PCR (see Table 1.2) was done to amplify the antibiotic neomycin resistance gene cassette from the plasmid mCherry2-N1 (Addgene, plasmid #54517) with flanking XbaI cut sites. The gene cassette was then PCR purified using the GeneJET PCR purification kit (ThermoFisher, Waltham, ON) and digested using the restriction enzyme XbaI (New England BioLabs, Whitby, ON). pLentiCRISPR_mCherry was also digested using XbaI. The digestion reaction consisted of 5 µL CutSmart® 10X buffer, 1 µL XbaI enzyme, 1 µg template DNA and topped to 50 µL final volume using diH_2O. The reaction tube was incubated at 37 °C

for 15 min and immediately heat-inactivated at 65 °C for 20 min. The digested gene cassette and vector were both PCR purified and ligated using T4 ligase. The ligated product was transformed by heat-shock procedures (42 °C, 1 min; on ice; 3 min) into a competent Stbl3 *E. coli* strain. The transformed product was grown on LB/kanamycin agar dishes and 3 colonies were picked and grown overnight before being DNA purified. This new assembly is thus named pLentiCRISPR_mCherry_NeoR to differentiate from the old one (see **Figure 2.2**).

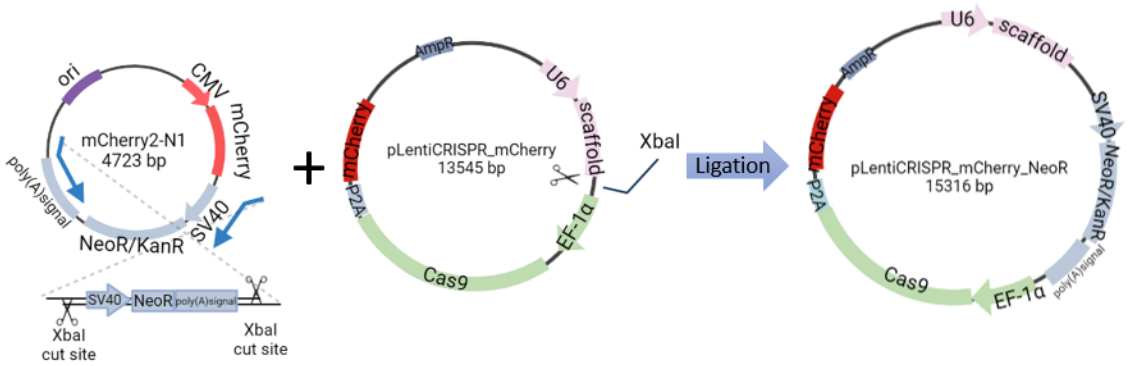

Figure 2.2 – Cloning procedure for pLentiCRISPR_mCherry_NeoR

Since the pLentiCRISPR_mCherry backbone is derived from LentiCRISPRv1, which LentiCRISPRv2 is also derived from, the vector backbone digestion, oligo annealing, and cloning procedures for the sgRNA insert were the same as in section 1.3. However, due to perhaps the pLentiCRISPR_mCherry being compromised from the start, it was not possible to continue with pLentiCRISPR_mCherry_NeoR. Hence, part of LentiCRISPRv2 was amplified to keep the inserted sgRNA and every other element needed for the transfer lentiviral plasmid except for the Cas9 gene cassette and the puromycin antibiotic resistance (see **Figure 2.3**). Part of pLentiCRISPR_mCherry_NeoR was amplified to keep the neomycin antibiotic resistance gene cassette and the Cas9 gene linked to an mCherry fluorescent reporter. LentiCRISPRv2 and pLentiCRISPR_mCherry_NeoR

were PCR amplified with Esp3I and EcoRI cut sites for correct orientation ligation using T4 ligase to produce pLentiCRISPR_mCherry_NeoRv2 (LCMNv2) (see Figure 1.2 and Table 1.2). The assembled products were transformed into a competent Stbl3 *E. coli* strain, colony PCR validated for the sgRNA insert, grown overnight and sent for sequencing verification by Sanger sequencing (Eurofins Genomics).

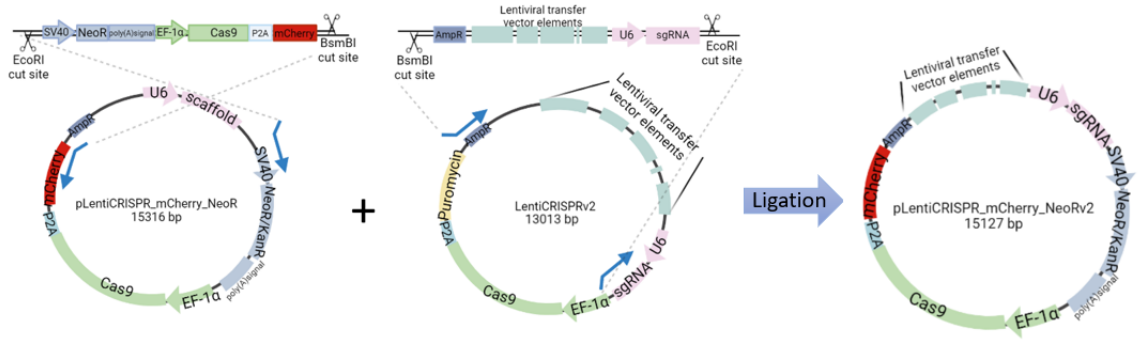

Figure 2.3 – Cloning procedure for pLentiCRISPR_mCherry_NeoRv2

2.6 Microscale cell culture and viral production and transduction

Cell culture: Before seeding cells onto DMF devices, all cell types (H1299, HEK293T, MCF-7, MDA-MB-231, and T47D-KBLuc) used in this study were grown in 100 mm petri dishes and were washed with 7 mL of PBS buffer, trypsinized with 430 µL of 0.25% trypsin-EDTA and suspended in 10 mL of complete medium (with heat-inactivated FBS). After centrifugation at 1,000 RPM for 5 min, the cell pellet was re-suspended in complete medium and cells were counted such that dilutions made would reach the required cell density. Aliquots of the cell suspension at densities (from ~1.0 x 10^6 to 2.5 x 10^6 cells/mL) were supplemented with 0.05% w/v Pluronics F-127.

For cell seeding of the target cells, we followed a similar protocol as described previously[31a]. Briefly, 1.5 µL of the above cell suspension was pipetted onto the bottom

plate at the edge of the top plate and loaded by applying driving potentials (2.5 V_{P-P} or ~500 V total, 15 kHz) into the appropriate reservoirs. 1.5 µL droplets were formed by elongating the liquid from the reservoir and activating the potential on an active dispensing electrode. The dispensed droplets from the reservoirs were actuated across a hydrophilic site (on the top plate) generating 1.5 µL and 1 µL volumes for eventual viral production and transduction respectively. Excess liquid from the spot was actuated to a waste reservoir and removed with a KimWipe. Viral production steps were then done immediately after cell seeding.

Viral production: HEK293T cells were seeded and cultured on the 1.6 mm diameter hydrophilic spot (following the *cell culture* protocol) at a suspension cell density of ~2.5 x 10^6 – 3.0 x 10^6 cells/mL. For viral production, we performed a reverse transfection protocol by first co-transfecting a mixture containing 0.75 µg of pMDLg/pRRE, 0.75 µg of pRSV-Rev, 1.5 µg of pMD2.g and 3 µg of the transfer vector pLv-mCherry with 12.5 µL of Lipofectamine 3000 and 12 µL of P3000 reagent for a total volume of 500 µL with Opti-MEM. After 20 min of incubation, 0.05% w/v of Pluronics F-127 were added to the mastermix to prepare for actuation on device. 1.5 µL of the Lipofectamine mastermix was actively dispensed and actuated towards the seeded HEK293T cells. The formulation (3µL total volume) was mixed in a circular fashion at the lentivirus production region by actuating adjacent electrodes (highlighted in the red box in **Figure 3.1a**).

Optimization of viral titers and transduction: HEK293T cells were seeded and cultured at the 'target cell' region at cell densities between 1-1.5 x 10^6 cells/mL following our *cell culture* protocol. After 24 h, four dilutions were generated containing the lentiviral particle-filled supernatant of the HEK293T cells at the production area. A dilution of 1:3

(DMEM : viral particles) was implemented by merging 1 µL of DMEM (10% heat-inactivated FBS, 8 µg/mL polybrene, 0.05% w/v Pluronics F-127; dispensed from the cell media reservoir) with 2 µL of the supernatant containing the viruses (**Appendix Figure S2.a**). 1 µL of the merged product was split and actuated to a 'target cell' region while the remainder (2 µL) was saved for the next dilutions. This procedure was repeated three times to generate dilutions 1:6, 1:12, and 1:24. Two additional spots were used for controls where cells at the same density were cultured with complete medium with 8 µg/mL polybrene on the first spot and without polybrene on the second spot. The device was flipped upside down and incubated overnight. After 24 and 48 h incubation, the device was imaged using an Olympus IX73 inverted microscope (Olympus Canada, Mississauga, ON, Canada) containing excitation and emission filters with wavelengths 585 nm and 608 nm respectively for mCherry fluorescence. We counted the fluorescent cells and estimated the viral titer using **Equation 1** (following Gill et al.[60]):

$$\frac{\#\ cells\ transduced\ \times\ \%fluorescent \times dilution\ factor}{transduction\ in\ volume}$$

$$= Transducing\ units\ per\ mL\ = (\frac{TU}{mL})$$

For CRISPR and shRNA optimization experiments, we followed the same procedures for *cell culturing, viral production,* and *optimization of viral titers*. The only changes to these procedures were the transfer plasmids were replaced with MISSION® shRNA plasmids (i.e. TRCN00000003300, non-target shRNA plasmid) and pLentiCRISPR-mCherry-NeoRv2 (LCMNv2) all-in-one Cas9 and sgRNA plasmids (Appendix Figure S1) for the shRNA and CRISPR experiments respectively.

Transfer: The next day, the transduced target cells were retrieved, pooled together with their corresponding dilutions 24 hours post-transduction. For example, 2 microwells that were subjected to the first serial dilution were pooled, 2 microwells that were subjected to the second serial dilution were pooled. The device was brought to a biological safety cabinet where the top-plate was taken apart from the bottom plate. 5 μL of PBS was pipetted onto the microwells and aspirated using a Pasteur pipette, leaving only adhered cells on the microwell. Cells were detached using 2 μL of trypsin-EDTA (0.25 % w/v) and the top-plate was placed back in the humidifying chamber, into the 37°C with 5 % CO_2 incubator for 2 min. Two microwells subjected to the same serial dilution from the same device were then pooled together by resuspending each microwell with 10 μL of complete medium and were added to 100 μL of complete media in a 96-well plate. The next day, the cultured wells were refreshed with complete medium supplemented with 1 μg/mL of puromycin for RNAi experiments and no antibiotics for CRISPR experiments. After seven days post-transduction, the cell lysate was collected for qRT-PCR assays or gene cleavage detection assays to verify gene knockouts.

2.7 Macroscale cell culture, transfection, viral production and transduction

Cell culture: H1299, HEK293T, MCF-7, MDA-MB-231, and T47D-KBLuc were grown in complete cell culture media formed from DMEM (4.5 g/L glucose, with L-glutamine, sodium pyruvate and phenol red) (HEK293T, MCF-7, MDA-MB-231) or RPMI 1640 with L-glutamine (H1299, T47D-KBLuc), supplemented with 10 % heat-inactivated fetal bovine serum. Cells were grown and maintained in 100 mm cell culture-treated petri dishes in an incubator at 37 °C with 5 % CO_2. For maintenance, cells were detached using a solution of trypsin-EDTA (0.25 % w/v) and resuspended in complete media and placed in

a 100 mm petri dish. Once detached, the cells were centrifuged at 1,000 RPM for 5 minutes and the supernatant was aspirated. The cells were then resuspended in fresh complete medium and counted using a hemocytometer for specific cell density seeding.

Transfection: Liposome-mediated transfection followed protocols described previously[31a]. 24-well plates were used for forward transfection experiments and 6-well plates were used when the assay was to be validated with Western blots or immunofluorescence. Thus, a scaling chart provided with the Lipofectamine 3000 reagent was used. Liposome-based transfection followed a 3-day timeline. Prior to transfection (day 0), cells were seeded at a density of 0.3 x 10^6 cells/mL in a 6-well plate until it reached ~70 % confluency. On day 1, 2.5 µg of DNA was pre-mixed with 5 µL of P3000 reagent in 125 µL of Opti-MEM and added to 11.25 µL of Lipofectamine 3000 reagent that was pre-mixed in 125 µL Opti-MEM. The lipid-DNA mixture was incubated at room temperature for 10 min, and then added to the cultured cells in the well-plate. On day 2 (after 24 h), the lipid-DNA complexes were removed from the wells by aspiration and fresh complete medium was replenished. Cells were stained with 1 µM Hoechst 33342 (Thermofisher, Waltham, MA, USA) (usually on day 3 or day 4) and incubated for 30 min for cell counting. Cells were imaged using a 20X objective on an Olympus IX73 inverted microscope (Olympus Canada, Mississauga, ON, Canada) that has fluorescence imaging capabilities (Hoechst: λ_{ex} = 350 nm and λ_{em} = 461 nm; GFP: λ_{ex} = 488 nm and λ_{em} = 509 nm; mCherry: λ_{ex} = 585 nm and λ_{em} = 608 nm). Fluorescence images were analyzed using an ImageJ pipeline.

Lentiviral production: To produce lentiviruses, two 10 cm petri dishes containing HEK293T cells were seeded at ~5 x 10^6 cells/mL to achieve ~80% confluency. Once

reached, the media was changed to fresh complete media and Lipofectamine 3000 transfection reagents were used. For each dish, 25 µL of Lipofectamine 3000 reagent was diluted in 475 µL of Opti-MEM medium with 1.5 µg of pMDLg/pRRE (Addgene, plasmid #12251), 1.5 µg of pRev (Addgene, plasmid #12253), 3 µg of pMD2.G (Addgene, plasmid #12259), and 6 µg of the transfer plasmid (pLv-mCherry - Addgene, plasmid #36084; non-target shRNA plasmid; ERα shRNA 1 (TRCN0000003300); LCMNv2_eGFP_12; LCMNv2_ESR1_76). Additional Opti-MEM medium was added to the mixture to top up the volume to 500 µL. The complete mixture was incubated for 20 min at room temperature before being added dropwise to the cells. After 24 h, the mixture in the dishes was removed and replaced with 6 mL of fresh complete media and incubated at 37 °C overnight.

After 24 h, the supernatant was collected in a 50 mL Falcon tube and was stored at 4°C until a second collection was made. Following another 24 h, a second collection of the supernatant was done, and the pH adjustment of the total supernatant volume was completed by adding HEPES (1.5 M, pH 7.5) in a 1:100 ratio. The supernatant was then filtered using a 0.45 µm polyethersulfone membrane filter (VWR, Mississauga, ON), and aliquoted into 1.5 mL Eppendorf tubes and stored at -80 °C.

Lentiviral titration: HeLa cells were seeded at a density of 4.0 x 10^4 cells/mL in 100 µL DMEM supplemented with 10 % FBS in a 96-well plate and incubated overnight at 37 °C and 5% CO_2. Prior to titration, DMEM supplemented with 10% heat-inactivated FBS and 4 ug/mL of polybrene known as the "diluent" were prepared. Serial dilutions (three 1:10 serial dilutions followed by seven 1:3 serial dilutions) were prepared in a 96-well plate where each lentiviral titer was titrated in duplicates (**Appendix Figure S2.b**). Each well

containing HeLa cells received 100 µL of the viral dilutions. After 24 h incubation, old viral media was discarded in bleach and 100 µL of fresh complete media without polybrene and containing 1 µg/mL of puromycin was added to each well and was refreshed each 2-3 days until 8-9 days. To estimate the transducing units (per mL), each well was washed twice with PBS and cells were stained with 0.1 % w/v crystal violet in 20% ethanol. After 10 min, the well plate was washed with water. Stained cells forming round colonies were counted and the transducing units per mL (TU/mL) were calculated as follows (**Equation 2**):

$$\frac{TU}{mL} = \frac{number\ of\ colonies}{total\ volume\ in\ well\ (mL)} \times final\ dilution\ factor$$

An alternative method for viral titration was used when a transfer plasmid did not contain a eukaryotic selection antibiotic resistance marker but instead a fluorescent marker (e.g., pLv-mCherry). We followed a protocol similar to Drayman and Oppenheim[61] which relied on measuring the viral titer using flow cytometry. HeLa cells were seeded on a 6-well plate at ~5 x 10^4 cells per well to reach a confluency of 40-50% the following day. Prior to the transduction, while the lentiviral particles were thawing on ice, DMEM (with 10% heat-inactivated FBS) was supplemented with 8 µg/mL of polybrene to use as a diluent for several dilutions. Following the template as seen in **Table 2.3** lentiviral dilutions were made and applied to their corresponding well in the 6-well plate.

Table 2.3 – 6-well plate template for lentiviral transduction for flow cytometry assessment of lentiviral titer

Lentiviruses: 100 µL Media: 400 µL	Lentiviruses: 50 µL Media: 450 µL	Lentiviruses: 25 µL Media: 475 µL

Lentiviruses: 12.5 µL Media: 487.5 µL	Lentiviruses: 6.25 µL Media: 493.75 µL	Lentiviruses: None Media: 500 µL

The plate was gently swirled by hand each 5 min for 30 min to ensure that all cells were coated with lentiviruses/media and returned to the incubator overnight with 5% CO_2 and at 37℃. 24 hours after the viral infection, 1.5 mL of normal complete media was added to each well and the cells were maintained for an additional two days until they were prepped for flow cytometry. For cell gating, each well was washed with 1 mL PBS and 150 µL of 0.25% trypsin-EDTA was used to detach the cells. The cells were collected in each their individual tube and washed with PBS again before centrifuging them at 1,000 RPM for 5 min. The supernatant was removed, and the cells were re-suspended in 3 mL of cell sorting buffer. The cells were then strained through a 40 µm cell strainer (VWR, Mississauga, ON), distributed into FACs sorting tubes (VWR, Mississauga, ON) and placed on ice until the BD FACs Melody (BD Biosciences) machine at Concordia's Genome Foundry was ready to be used. The cells were then gated for the percentage of mCherry positive cells. To determine the viral titer (TU/mL), **Equation 1** was used.

Transduction: For viral transduction of target cells, we followed a protocol similar to Li and Rossi which the company Sigma-Aldrich relied on for transducing MISSION® plasmid packaged lentiviral particles[62]. 1.6×10^4 cells of target cells per well were seeded in a 96-well plate and then incubated overnight at 37℃ and with 5% CO_2. After 24 h, the media was removed from the wells and replaced with 100 µL of media containing polybrene (8 µg/mL) for each well. Next, a determined volume of lentiviral particles of known titer was added to the appropriate wells. The plate was gently rocked by hand and

then incubated overnight. The determined volume of lentiviral particles is calculated upon the multiplicity of infection (MOI) decided to use. The following **Equation 3** was used to know the volume of viral stock to use based on the MOI:

$$\frac{MOI \times total\ cell\ number}{Viral\ titer} = volume\ of\ viral\ stock\ to\ use \text{ (in mL)}$$

where MOI = TU/cell and viral titer = TU/mL

After 72 h, the medium containing lentiviral particles was removed and 100 µL of fresh media was added to each well. Images of the cells were taken with a fluorescent microscope and quantification was done with ImageJ.

RNAi and CRISPR experiments: Before transduction, target cells were seeded at a cell density of 1.6 x 10^4 cells/mL in a 96-well plate. After 24 h, the cells were infected with shRNA-packaged or all-in-one Cas9 and sgRNA- packaged lentiviruses at an approximate MOIs of 0.5, 1, 2 and 10. Target cells were maintained for 7 days while refreshing the medium (RNAi: supplemented with 1 µg/mL of puromycin, CRISPR-Cas9: no antibiotics) every two days. After 7 days, the cells were collected by lysing them with 50 µL of DNase/lysis solution for qRT-PCR validation or lysing them with 52 µL of cell lysis buffer (50 µL lysis buffer and 2 µL protein degrader solution) for genomic cleavage detection assays.

2.8 qRT-PCR

Gene-specific primers were designed on Benchling (**Table 2.4**) and ordered via Biocorps (Montréal, QC). Cell lysis was performed as described in the manufacturer's Cells-to-C_T™ 1-Step *Power*SYBR® Green kit protocol (ThermoFisher, Waltham, ON). Cell medium was removed, and the cells were washed with ice-cold PBS buffer. After

aspiration of PBS, 50 µL of room-temperature DNase/lysis solution was added and mixed to each well. The well plate was incubated at room temperature for 5 mins and 5 µL of room-temperature stop solution was then added. The well plate was incubated for another 2 min at room temperature and then the lysates were placed on ice for the next step. The RT-PCR master mix was prepared on ice which consisted of 10 µL of Power qRT-PCR mix, 0.16 µL Power RT mix, 2 µL of the gene-specific forward and reverse primer (10 µM) and nuclease-free water up to 18 µL. The appropriate volume of qRT-PCR master mix and lysate were added to a 48-array plate. The reactions were run in the ECO real-time PCR machine (Illumina) at the following conditions: reverse transcription (1 cycle, 48°C, 30 min), polymerase activation (1 cycle, 95°C, 10 min), amplification (40 cycles; 95°C, 15 sec; 60°C, 1 min) and melt curve step (1 cycle; 95°C, 15 sec; 60°C, 15 sec; 95°C, 15 sec). Data produced from the qt-PCR reactions were further analyzed using the ECO software provided with the ECO system.

Table 2.4 – **Primers used for qRT-PCR**

Gene-specific primers	Sequence (5'-3')
ERα - Forward	TTGACCCTCCATGATCAGGTC
ERα - Reverse	GCAAACAGTAGCTTCCCTGG
β-actin - (Forward & reverse)	Proprietary (ThermoFisher)

2.9 Gene cleavage detection assay

To validate CRISPR-Cas9 knock-outs, the gene cleavage detection assay was done with the GeneArt genomic cleavage detection kit (Thermofisher). After performing CRISPR assays, the cells were collected and lysed with 50 µL of the provided lysis buffer and 2 µL of protein degrader solution. Once lysed, the whole cell lysate mix was transferred into a PCR tube for the following thermocycler conditions: 68°C for 15 min, 95°C for 10 min and 4°C on hold. The reaction was then PCR amplified (see Table 1.5) for the region of interest where the CRISPR-Cas9 cut has occurred. One PCR reaction consisted of 2 µL of cell lysate, 1 µL of forward and reverse primers mix (10 µM), 25 µL of provided AmpliTaq® Gold 360 Master mix and 25 µL of diH_2O. The following parameters were used for the thermocyler run: enzyme activation (1 cycle, 95°C, 10 min), 35 cycles of denaturation (95°C, 30 sec), annealing (57°C, 30 sec) and extension (72°C, 30 sec), a final extension (72°C, 7 min) and finally infinite hold at 4°C. The PCR product was then run on a 0.8% gel at 130 V for 30 min to verify that the correct amplicon was present. The cleavage assay was first set up by purifying the PCR product and then by denaturing and re-annealing the PCR fragments to form heterogenous DNA duplexed. Briefly, 200 ng of PCR product was combined with 1 µL 10X detection reaction buffer in a PCR tube. The volume was then brought to a total of 9 µL with water. The PCR tube was placed in a thermocycler for the following run: 95°C for 5 min, 95°C-85°C for a ramping of -2°C/sec, 85°C-25°C for a ramping of -0.1°C/sec and finally 4°C on hold. The next step consisted of cleaving the heteroduplex DNA containing the indel with the detection enzyme. For this, 1 µL of detection enzyme was added to the previous PCR tubes to have a total reaction volume of 10 µL. The reaction was incubated at 37°C for one hour and then was

immediately ran on a 2% gel using lithium acetate borate (LAB) buffer at 220 V for 20 min. Finally, the gel was scanned using a UV transilluminator and the imaging system ImageJ was used to determine the relative proportion of DNA contained in each band to calculate the cleavage efficiency (see **Equation 4** below).

$$Cleavage\ efficiency = 1 - [(1 - fraction\ cleaved)^{1/2}]$$

Table 2.5 – **Primers used for gene cleavage detection assays.**

Gene target amplification – primer	Sequence (5'-3')	Product size (bp)	Expected cleaved bands' size (bp)
eGFP - Forward	GCCTCTGCCTCTGAGCTATTC	433	293 & 160
eGFP - Reverse	TGAAGAAGATGGTGCGCTCC		
ERα - Forward	CATGACCCTCCACACCAAAG	409	235 & 174
ERα - Reverse	TTCTCCAGGTAGTAGGGCAC		

2.10 Imaging pipeline on ImageJ

Images that were taken via microscopy were acquired using a Hamamatsu digital camera (Model C1140-42U) with the HCImageLive software. The images were then processed using ImageJ using a protocol similar to previous work[31a]. For each image, the channels were split, and their brightness and contrast were adjusted for clear identification of the cells against the background. The image was then duplicated for processing and the threshold was adjusted to turn the duplicated item into a black and white image. The cells were identified by using the 'analyze particles' feature with 'outlines' chosen in the settings

which will open a new window showing a summary of the count of particles (cells), along with the total area and the average size number. To measure the percentage of fluorescent cells, the following **Equation 5** was used:

$$\%\ Fluorescence = \left(\frac{mCherry\ positive\ cells}{Hoechst\ stained\ cell}\right) \times 100$$

Chapter 3. Results and Discussion

This section presents my results in characterizing and validating the lentiviral generation, packaging, and transduction platform. The device optimization, the characterization of the platform for lentiviral generation, and the validation work for knocking out and knocking down a receptor in a breast cancer cell line are presented.

3.1 Lentiviral generation (LENGEN): Digital microfluidics for viral production and transduction

Techniques like gene silencing or gene-editing requires considerable efforts in developing efficient tools to deliver the genetic cargo that will enable the regulation of gene expression and interrogate the function of a gene either at the genetic or translational level. For example, the use of viral-derived vectors enables the efficient uptake of biological agents such as DNA, mRNA, and proteins.[63] However, the process to produce and to transduce these viral vectors are costly, extremely labor-intensive and overall very time-consuming. The overall goal of this work was to address the challenges of automating the production and the transduction of viral-based carriers for typical biological agents.

As shown in **Figure 3.1a**, a device was designed to automate the production and the transduction of viral-derived vectors. Several design iterations were required to develop a device that is capable of producing and transducing virus particles. Two challenges were encountered in the process, including (1) generating the highest lentiviral titers that will enable efficient transduction and (2) to multiplex viral transduction analysis on-chip. These challenges called for several innovations with the device design. First, to package and to produce lentiviruses, it requires a host (e.g., HEK293T cells) that is easily transfected and supports high-level of expression of the viral proteins to allow for

producing the highest possible lentiviral titers. To enable such a process, we fabricated hydrophilic sites that are patterned on the device top-plate to serve as sites for cell seeding and proliferation. These sites enable procedures called "passive dispensing" (similar to exchange media for continuous culture, to produce and to deliver lentiviral particles. In initial experiments, we used a previous device design that cultured cells on ~1.2 mm diameter hydrophilic sites which enabled lipofection-mediated transfection with high efficiency[31a]. However, using this device we observed: (1) the production of the lentiviral titers generated very low or 0% transduction efficiency and (2) the electrode configuration made it difficult to mix droplets containing the DNA and lipids resulting in uneven distribution of viral particles when harvesting the virus from the generation site. We hypothesize that the low transduction efficiency is due to the low cell density (corresponding to lower viral titers) and therefore we created a larger cell culture site (~1.6 mm dia.) that houses ~ 2 500 cells at the optimal 50-70% confluency. In addition, we created a four-prong electrode system (highlighted as the 'production area') that is directed towards the hydrophilic site. The latter innovation was particularly important for reliable droplet mixing and splitting since the droplet is continuously circulated around the four-prong electrode to facilitate uniform mixing and is easily extended to facilitate "necking" during droplet splitting. To fulfill the multiplexing capabilities, the device design contains a 'highway' track to enable one-directional movement towards the cell-culturing site, and the delivery of the generated lentiviral particles to several cell-culturing sites. Generally, flat square or inter-digitated electrodes are used to facilitate the droplet operations on a digital microfluidic device.[31a, 50c, 64] These types of electrodes require complicated wiring schemes that can be difficult to design as we increase the electrode density (unless you use

multi-layer fabrication techniques[65]). Instead, we modified the electrode design such that the droplet only moves towards the overlapping "prong"-electrodes (**Figure 3.1b)**. Using such a design allows the electrodes to be bussed through a minimal two connections – i.e. on our device design we connected 22 electrodes using 2 connections (which we call the "highway track") – which allowed us to increase the number of replicates that can be performed on the device. Moreover, the reduction in connections enabled us to incorporate a symmetrical design on the device to allow 12 transduction assays to be conducted simultaneously. We anticipate that future designs can use such electrode designs to overcome multiplexing challenges that is commonly associated with digital microfluidics.

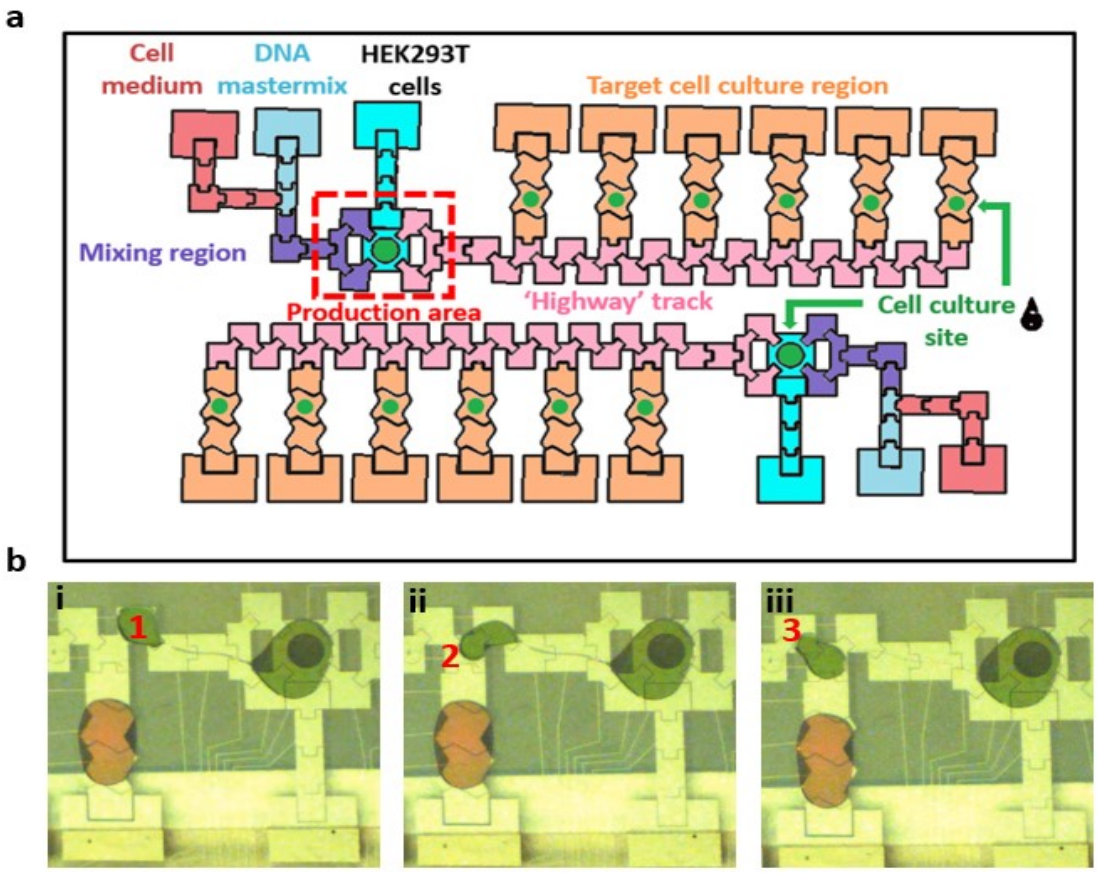

Figure 3.1 - LENtiviral GENeration, packaging, transduction, and analysis (LENGEN) on a digital microfluidic platform. *(a) Top-view schematic representation*

of the LENGEN device. The bottom plate contains two sets of 139 electrodes each for lentiviral generation and packaging, cell culturing, transduction, and analysis. For each set, there is one patterned 1.6 mm dia. cell culture site for production and six ~1.2 mm dia. site for transduction and analysis. The production area houses a 3 μL droplet which is split into unit droplets (~ 1 μL) that covers the area of an electrode and actuated to the cell culturing sites. Two sets of electrodes enable replicates or different conditions to be performed in parallel. (b) Frames from a movie depicting (i) the droplet resting on electrode 1, (ii) droplet moves to electrode 2 when it is activated and (iii) droplet shows uni-directional movement onto electrode 3 (and not electrode 1) when electrodes 1 and 3 are bussed. The "highway track" of electrodes is used to enable delivery of the lentiviral particles to the cells with minimal electrode connections and to provide multiplexing capabilities on digital microfluidic devices.

With this configuration, a five-step procedure was developed to facilitate the automation of the generation, packaging and the delivery of the virus system. The schematic shows the events at the genetic level with an image-based representation of what is occurring on device. As shown in **Figure 3.2**, the producer cells (HEK293T) are in suspension and actuated to the production area by loading and dispensing from reservoirs. In step (ii), a unit droplet of liposomes and viral DNA plasmids (pMDLg/pRRE, pRev, pMD2.G and transfer plasmid of interest) are dispensed and merged followed by continuously circulation in the production area containing 8 electrodes. In step (iii-iv), the Lipofectamine mixture is actuated to the HEK293T cells and mixed together to replicate the reverse transfection procedure [66] on device (i.e. transfecting unseeded cells as opposed to overlaying transfection complexes onto seeded cells). Finally, in step (v), after 24 h, the lentiviral particles are produced in the supernatant (cells are adhered to the hydrophilic spot) and serial dilutions (1:3, 1:6, 1:12, and 1:24) are formed to infect target cells following the procedure shown in Appendix **Figure S2.a** (see Methodology section 2.6 for more details). This LENGEN device for lentiviral generation: production and transduction,

is the first (to our knowledge) that is capable of automating the procedures of preparation, production, and transduction with viral-derived vectors.

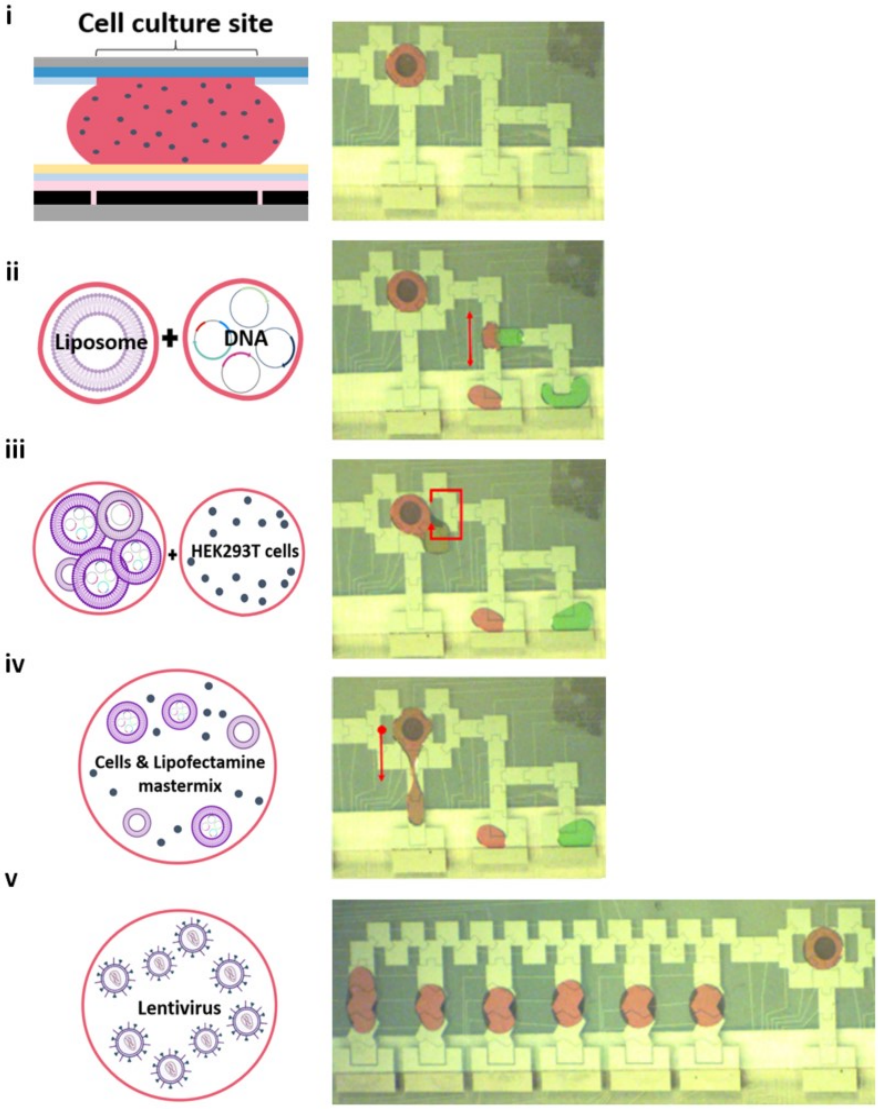

Figure 3.2 - Lentiviral production and transduction strategy on the LENGEN platform. *Left: the graphical representation of the five-step lentiviral generation, production, transduction, and analysis. Right: images from a movie for each of the five steps. Coloured food dyes were used to show the droplet. Step (i) HEK293T cells in a droplet are seeded at the production region. (ii) Plasmids and lipids from separate reservoirs are dispensed and merged and incubated for 20 mins. (iii) The DNA and lipids are dispensed into the HEK293T cell culture region and are mixed in a circular fashion around the adjacent electrodes. (iv) Excess mixture (containing plasmid, lipids, media) is dispensed away from the HEK293T cell culture region for removal. (v) After seeding the target cell line at the cell culture regions, unit droplets containing lentiviral particles with*

the plasmid of interest is split from the production region and actuated to a cell culture region (transduction). Analysis of the cells can be performed via microscopy after 24 or 48 h. For transduction analysis, cells can be removed by trypsin and cultured in well-plates for verification analysis (e.g., RT-PCR, gene cleavage) or for sorting and isoclonal expansion (not shown).

Breast cancer cell lines (MCF-7 and T47DKB-Luc) were chosen as models for our lentiviral study to show that our automated platform can genetically modify oncogenes and use this method to potentially find therapeutic targets against these genes.[67] For all results described here, a droplet comprised of the breast cancer cells (at various cell densities) were loaded into the reservoirs. These droplets were dispensed into smaller volumes and actuated towards the cell culturing sites using passive dispensing techniques (as described above). Two parameters were evaluated – cell viability and transduction efficiency. As described in the Appendix **Figure S3**, both cell lines were viable on the device and showed comparable viability when cultured in well-plates. We also evaluated the cell viability after 48 and 72 h (since the gene knockouts after lentiviral transduction occurs within this timeframe[30, 68]) and we observed an average viability 89.5, 83.7, 85.7 % for MCF-7 and 98.8, 98.4, 88.6 % for T47DKB-Luc on the device respectively. **Figure 3.3a** shows representative fluorescently labeled images of the MCF-7 and T47DKB-Luc cells, and as shown, the cells are proliferative, and the morphologies of the cultured breast cancer cells were similar to the cells cultured in well-plates (**Figure S3c-d**). An additional assay was developed to determine the transduction efficiency on device by seeding T47DKB-Luc cells on the cell culturing sites. As shown in **Figure 3.3b**, the efficiency is ~43.0 % at day 2 post-transduction and improves to ~60.1% at day 4 post-transduction. These efficiencies are also a significant improvement from lipid-based transfection, achieving at best ~14 % at 7.5 x 10^5 cells/mL after day 1 (see **Figure S4**). This is a trend usually observed for hard-to-transfect cell lines like T47DKB-Luc.[69]

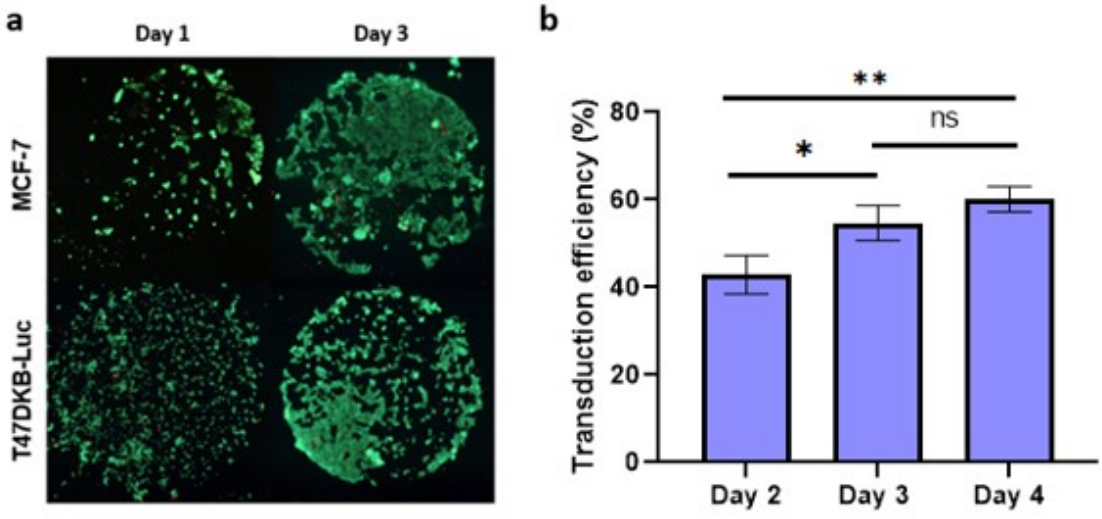

Figure 3.3 - Optimizing viability and transduction efficiency for breast-cancer cell lines (MCF-7 and T47DKB-Luc) on the LENGEN device. *(a) Fluorescent images of each cell line treated with fluorescein diacetate (green) stains live cells and propidium iodine (red) stains for dead cells on the cell culturing sites for day 1 and 3. (b) Graph showing the transduction efficiency on T47DKB-Luc with a pLV-mCherry plasmid on the LENGEN platform for days 2-4. A student's t-test ($P < 0.05$) was used to evaluate the significance (* for a $P \leq 0.05$, ** for a $P \leq 0.01$ and ns for $P > 0.05$) between each day. Error bars represent ± 1 S.D. with $N = 3$.*

From literature, a critical factor to determine successful lentiviral transduction is the functional titer, which is the smallest transduction unit of virus capable of infecting cells and expressing the transgene.[27, 70] Hence, we performed four serial dilutions of the lentiviral particles containing a non-targeting mCherry plasmid to help determine the optimal concentration of functional lentiviral required in HEK293T cells. A number of mCherry transduced cells were counted (using imaging techniques - see **Figure 3.4a**) on the hydrophilic spot after 24 h and 48 h (**Figure 3.4b**). Generally, as shown, the most optimal concentration of lentiviral particles was observed after 48 h transduction - achieving a range 6.5 x 10^6 to 1.33 x $10^{\wedge 7}$ TU/mL with the 1:3 dilution resulting in the highest fluorescence. These values were also translated to a viral titer (using Equation 1) and it was determined that on-device, we are able to obtain a functional titer of > 5 x 10^6

or 1 x 10^7 TU/mL after 24 or 48 h respectively (**Figure 3.4c**) - values very similar to titers obtained from benchtop methods[71]. We also calculated the amount of transducing units generated per cell on the device and compared to macroscale techniques. On average, we are able to produce 1.56 TU/cell and 2.65 TU/cell on device after 24 and 48 h respectively, which is very similar to the benchtop after 5 days of harvesting (2.80 TU/cell) (**Figure 3.4d** and **S5**). In practice, it was decided that 24 h post-transduction step was sufficient for the gene silencing and editing assays since it resulted in titers that are sufficient for observing knockdown and knockout events.

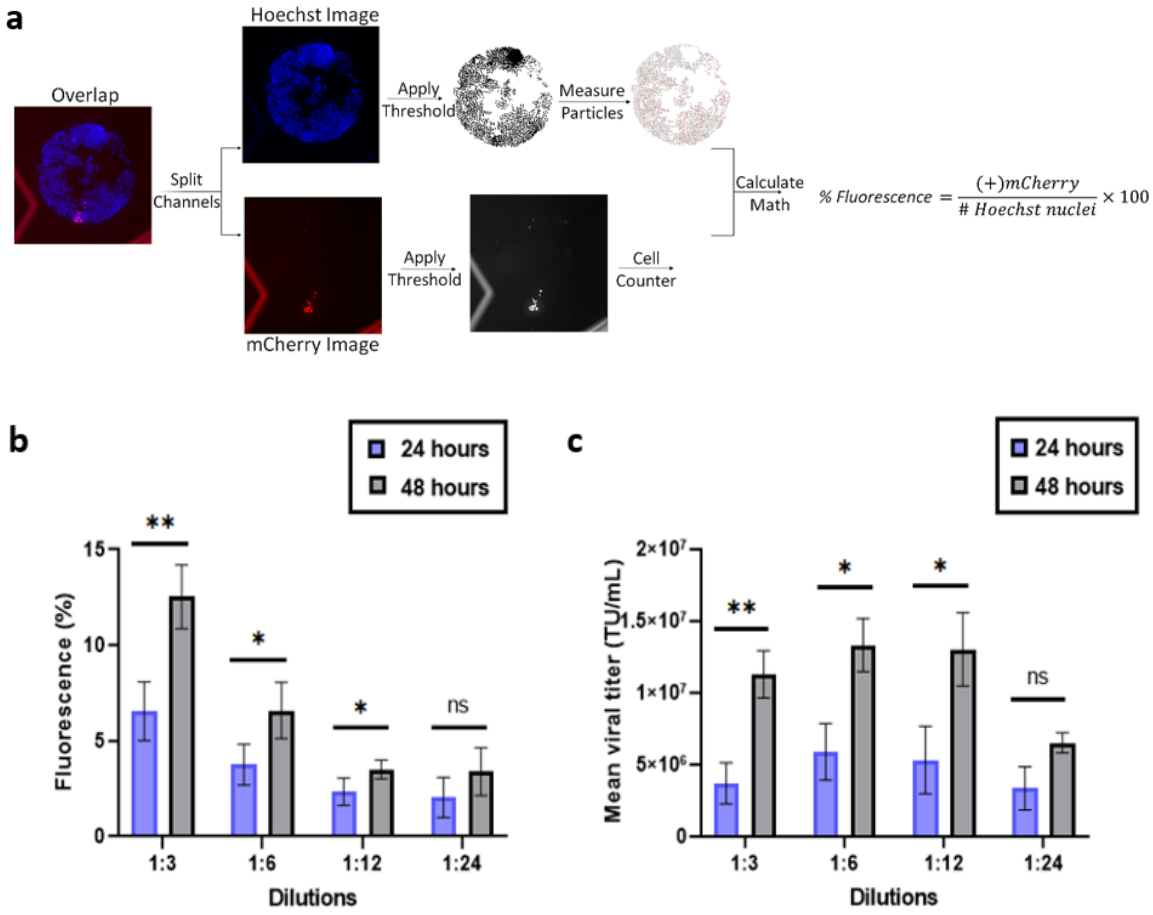

d

Microscale (24 hours)		Microscale (48 hours)		Macroscale (5 days)	
Dilutions	TU/cell	Dilutions	TU/cell	Dilution	TU/cell
1:03	1.23	1:03	3.55	3:10	2.81
1:06	1.92	1:06	2.60	2:10	2.73
1:12	1.77	1:12	2.30	1:10	1.95
1:24	1.33	1:24	2.13	0.5:10	3.73
Average	1.56	Average	2.65	Average	2.80

Figure 3.4 - Optimizing lentiviral production. *Schematic (a) showing the imaging pipeline used to analyze fluorescence percentage of mCherry positive cells. (b) and (c) plots are showing the (b) fluorescence efficiency, (c) mean viral titer as a function of supernatant dilutions (1:3, 1:6, 1:12, and 1:24) for positive mCherry HEK293T cells after 24 and 48 h lentiviral production and transduction. (d) Comparison of the amount of transducing unit produced per cell on microscale and macroscale. For (a), the schematic is showing the workflow to calculate the % fluorescence (of mCherry) after viral transduction. Mean viral titer can then be calclated using Equation 1. For (b), positive mCherry cells were counted and divided by non-transduced mCherry cells. For (c), the estimated mean viral titer amount was calculated by multiplying the number of cells transduced with the percentage of fluorescence, dilution factor, and dividing the total by the volume of lentiviral particles used for transduction (i.e. transducing units (TU) per milliliter). For (d), a sample calculation on how TU/cell was obtained are shown in Supplementary Figure S5. A student's t-test ($P < 0.05$) was used to evaluate the significance (* for a $P \leq 0.05$, ** for a $P \leq 0.01$ and ns for $P > 0.05$) between the dilutions. Error bars for both plots represent ± 1 S.D. with $N = 3$.*

Other factors that affect the transduction efficiency are the size of the lentiviral payload[72] and cell-type[73]. Since shRNA and CRISPR vectors are usually ~ 15.0 kb in size (compared to smaller ~ 4.7 kb plasmids containing fluorescent reporter mCherry), we used the system above to evaluate the effects of the lentiviral payload of ~15.0 kb (using LCMNv2 – see **Figure S1**) in hard-to-transfect cell lines like H1299 and T47DKb-Luc. As shown in **Figure 3.5a**, we obtained the highest for the 1:3 dilution which correspond to ~ 10.8 % of H1299 cells that show mCherry fluorescence. Comparatively to H1299,

T47DKb-Luc had higher transduction efficiency with the 1:6 dilution. In **Figure 3.5b**, T47DKB-Luc highest transduction efficiency was ~ 5 % which is similar to what is obtained in literature [74]. It is generally observed that larger lentiviral payloads will lead to lower transduction efficiency[75], but there is no clear mechanism to predict which cell line will transduce more efficiently[76]. However, the results do suggest that for a particular cell type there should be focus on optimizing MOIs or lentiviral dilutions and post-infection incubation times to obtain effective transduction. In the future, it may be important to further to study different strategies[77] for effective transduction of lentiviral particles especially if the application calls for a wide variety of cell types (immortalized, primary, stem, etc…).

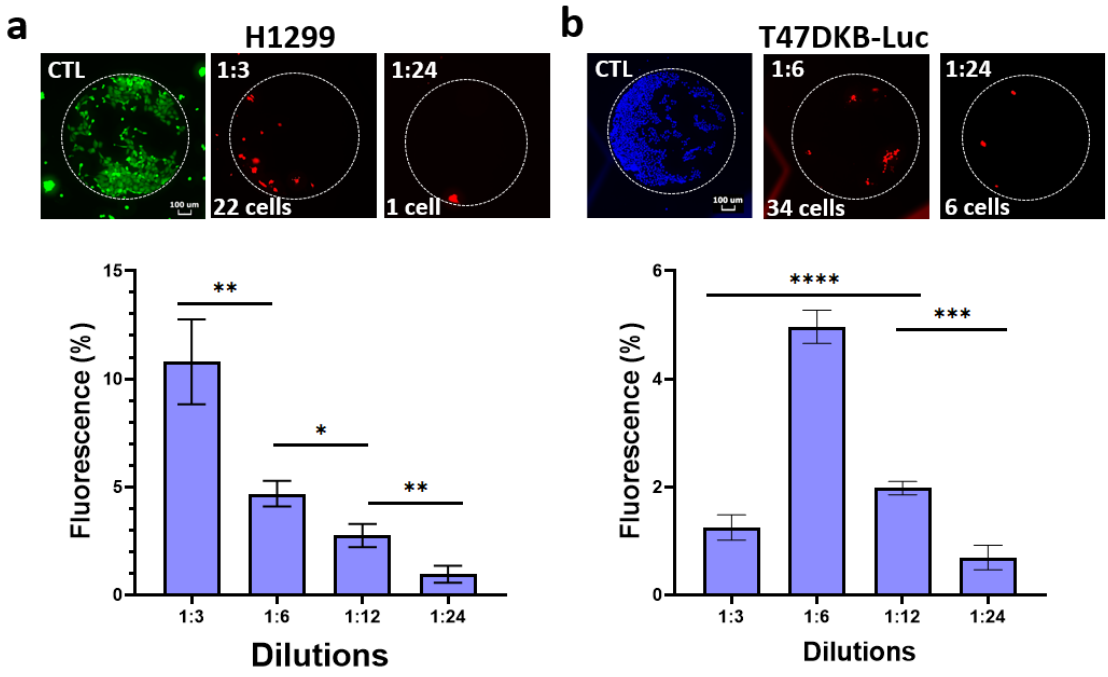

Figure 3.5 - Evaluating the effect of a large lentiviral payload (~15 kb) for different cell lines: (a) H1299 and (b) T47DKb-Luc. *Each plot is accompanied with pictures showing the cells seeded on the hydrophilic spot (white outline) situated on the LENGEN device. Wild-type H1299 cells contained eGFP integrated into the cells (from Genecopeia) and wild-type T47DKb-Luc were fluorescently labeled with Hoechst 33342 stain. All cells were transduced with the lentiviral particles (at different dilutions 1:3, 1:6, 1:12, and 1:24) containing an mCherry fluorescent reporter. (+)mCherry cells were counted to generate the % fluorescence efficiency. A student t-test ($P < 0.05$) was used to evaluate the*

*significance (shown as * for a P ≤ 0.05, ** for a P ≤ 0.01, *** for a P ≤ 0.001, **** for a P ≤ 0.0001) between the dilutions. Error bars for both plots represent ± 1 S.D. with N = 3.*

3.2 LENGEN for lentiviral knockdown and knockout assays

To evaluate the potential of our system for knockdown and knockout assays, we packaged shRNA and CRISPR plasmids that will target estrogen receptors in breast cancer cells. Approximately 70 % of breast cancer tumors express the estrogen receptor alpha (ESR1) since they control a range of physiological processes in regulation and development of the female reproductive system.[78] Thus, there is much interest to systematically investigate genes whose loss affects cell growth or increases the estrogen-independent growth of ER+ breast cancer cells.[79] In this part of the work, we applied our system to automate the process of producing and transducing the lentiviral particles containing the ESR1 target and examining the knockdown (shRNA) or knockout (CRISPR) of the target gene.

To test the effectiveness of our method for gene expression analysis, RNAi assays were performed on the LENGEN device (**Figure 3.1**). The transfer plasmid targeting the ESR1 are packaged and produced using HEK293T cells and the supernatant are diluted to different viral concentrations (1:3, 1:6, 1:12, 1:24) (replicating different MOIs) which are used to transduce MCF-7 cells. Expression values from LENGEN protocols were obtained by qRT-PCR[80] methods by removing the top-plate containing the transduced cells from the DMF device (via trypsinization) and transferring the cell to well-plates for analysis after outgrowth of seven days (see section 2.6 *Transfer*). These data, for high dilutions (1:24) and low dilutions (1:3), the relative reduction in gene knockdown is 18 ± 8.8 and 89

± 37.6 % respectively (**Figure 3.6a**) and is similarly observed in lentiviral well-plate conditions (**Figure 3.6b**). The gene expression percentages for both LENGEN and standard conditions were confirmed by a $\Delta\Delta C_q$ method[81] (see **Figure S6** for qPCR curves) which confirm that our LENGEN method is capable of gene silencing.

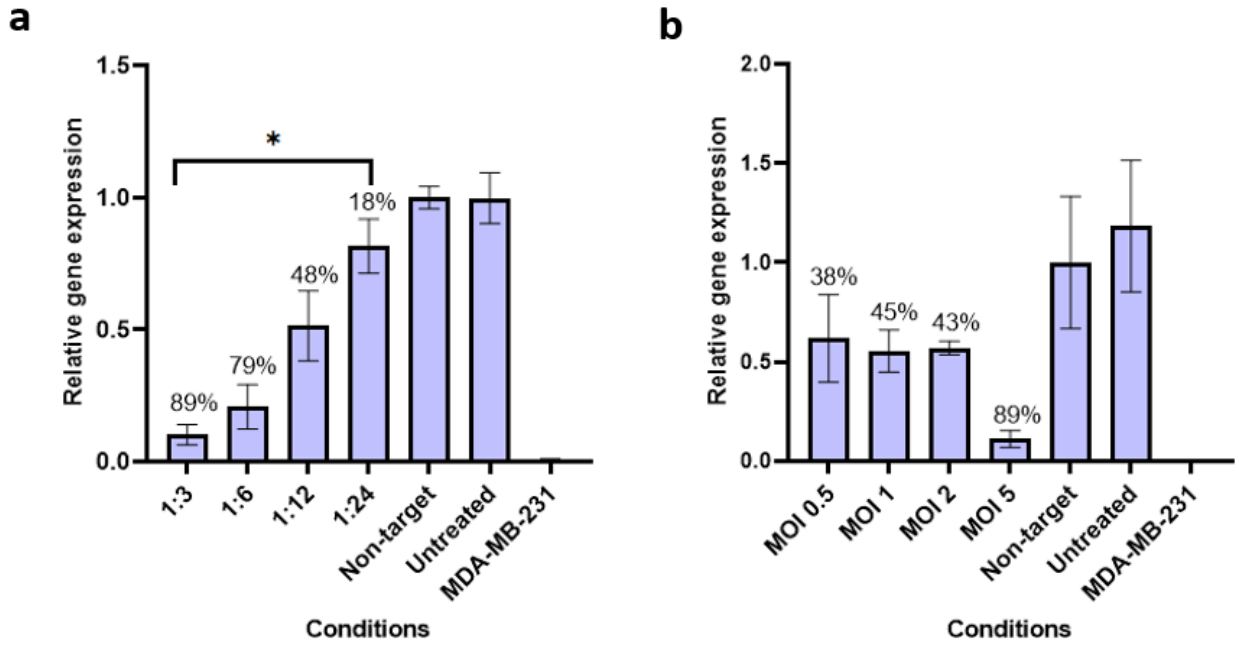

Figure 3.6 - shRNA knockdown assays for ESR1. *Evaluating the relative gene expression of Estrogen Receptor 1 (ESR1) in MCF-7 cells that were performed in (a) LENGEN device and (b) well-plates. We generated, packaged lentiviral particles containing shRNAs targeting ESR1 and transduced them in MCF-7 cells. shRNA-mediated silencing of ESR1 was assessed using a ΔΔCq method to determine relative gene expression from qRT-PCR data with ACTB (β-actin) as an endogenous reference gene. The cells exhibited MOI-dependent viral delivery of shRNA#1 targeting ESR1 knockdown, with mRNA reduction by 38%, 45%, 43% and 89% when cells were treated with MOI of 0.5, 1, 2 and 5 respectively. In the case with LENGEN, the cells exhibited dilution-dependent viral delivery of shRNA#1 targeting ESR1 knockdown, with mRNA reduction by 89%, 79%, 48% and 18% when cells were treated with dilutions 1:3, 1:6, 1:12 and 1:24 respectively. Significance between dilutions 1:3 and 1:24 is significant (shown as * for $P \leq 0.05$). Comparison of non-targeting shRNA to untreated samples shows no significant effect on gene expression. A negative control depicts ESR1's relative downregulated (almost zero expression levels) expression in MDA-MB-231 cells. Error bars for both plots represent ± 1 S.D. with N = 3.*

The knockout assay was motivated by the wide-spread interest in using CRISPR for identifying essential genes related to cancer and other diseases.[22a, 82] Once again, MCF-7 cells were seeded, grown, and transduced by a dilution series (generated on-chip) of lentiviruses containing an all-in-one plasmid with the Cas9 gene cassette and a sgRNA guide targeting ESR1. As shown in **Figure 3.7a**, the trend is very similar to what is observed with the RNAi experiments – at lower dilutions, we observed significant reduced fluorescence compared to the higher dilutions, thus reduced transgene expression - and this trend was identical to that observed in standard conditions (**Figure 3.7b**) and in literature[83]. To verify the knockout, we performed downstream analysis by removing the MCF-7 cells from the device and culturing them in well-plates (see section 2.6 *Transfer*) in preparation for a genomic cleavage assay[22b] (**Figure 3.7c**). The band patterns are similar to what is observed in the genomic cleavage gel from MCF-7 cells transduced in well-plates at different MOIs (**Figure 3.7d**). Since genome editing efficiency varies with different cell lines[84], we implemented the gene-editing workflow[22b] on H1299 cells (i.e. non-breast cancer cells) and similarly observed successful knockout of integrated eGFP (**Figure S7**). Although downstream gene editing analysis of CRISPR knockouts from microfluidic devices have been shown previously[45, 57b, 85], this is the first demonstration showing integration of lentiviral packaging, generation, and transduction on a microfluidic device followed by downstream gene editing analysis (off-device).

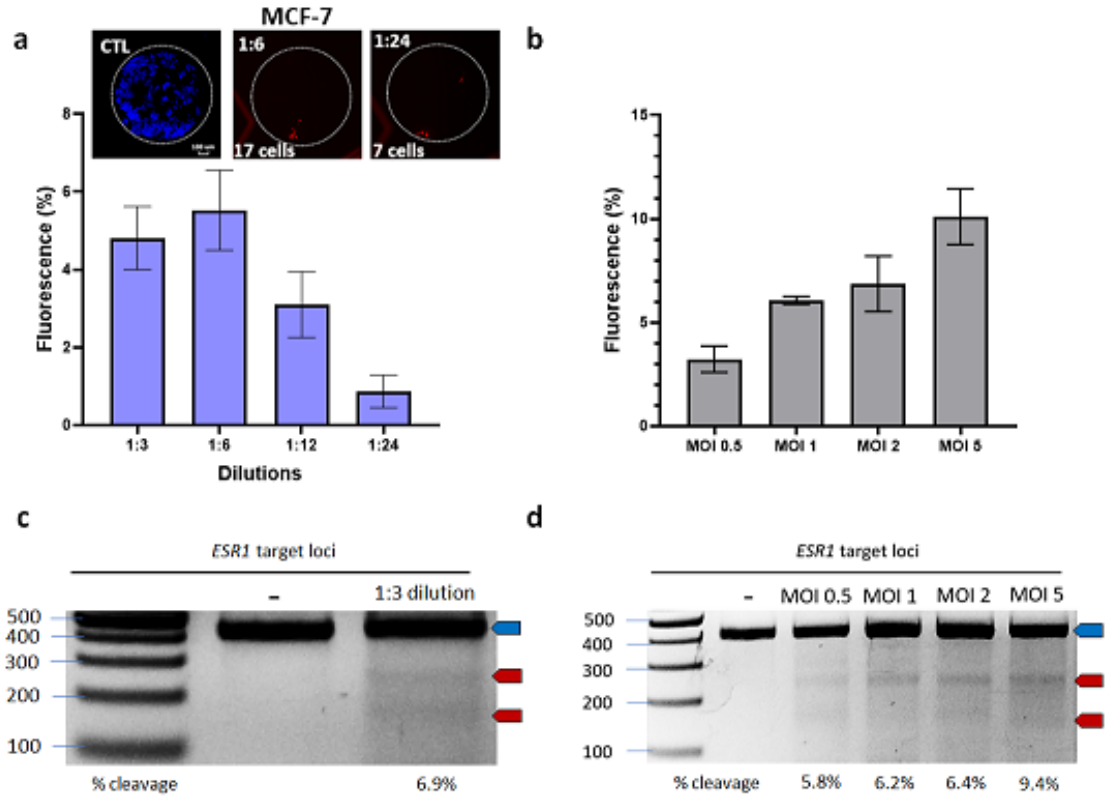

Figure 3.7 - Knockout assays for ESR1. *Evaluating the knockout efficiency of ESR1 in MCF-7 cells performed in well-plates and on LENGEN. Lentiviral particles containing all-in-one Cas9/sgRNA targeting ESR1 were generated, packaged, and transduced using (a) LENGEN or (b) well-plate protocols. Plots of fluorescence efficiency were measured at (a) different MOIs (0.5, 1, 2 and 5) and (b) different dilutions (1:3, 1:6, 1:12, 1:24) with cell images showing Hoechst 33342 stained wild-type MCF-7 cells or transduced (+)mCherry cells. (c-d) Each transduction was verified by a genomic cleavage assay after seven days post-transduction. The parental band is 409 bp (shown by the blue arrow arrow) and the cleavage bands are 235 bp and 174 bp (shown by red arrows). Following LENGEN protocols, cells were removed from the top-plate, transferred to a well-plate, and the 1:3 transduced cells were pooled together to perform the genomic cleavage assay. Error bars for both plots represent ± 1 S.D. with N = 3.*

As depicted in **Figure 3.1**, this method was carried out in a 12-plex format (through the use of "highway tracks") and we propose that this will be straightforward to expand this technique to much higher levels of multiplexing given the electrode and bussing techniques presented here (and particularly with recent reports of active matrix methods[65, 86]). In addition, through the use of DMF for lentiviral packaging, production, and transduction, it is possible to obtain very similar gene expression profiles (via RNAi and

CRISPR techniques) to that obtained of benchtop assays, while enabling 100-fold reduction in volumes to save precious lentiviral samples. This is an advantage because current practices of lentiviral production require high concentration of lentiviruses to reduce infection volumes to target cells but the conventional cell culture platforms do not allow for further reduction of these infection volumes. In particular, when it comes to generating very concentrated amounts of viral titer, several days of lentiviral harvests within large batches of culture and rounds of ultracentrifugation are necessary to achieve a desirable concentration. Thus, with our platform, the time for lentiviral packaging, production and transduction of target cells has substantially decreased from generally two weeks [30, 87] to 2 days and therefore reducing the tedium needed for packaging and producing (and transducing) lentiviruses.

Chapter 4. Concluding Remarks and a Future Perspective

A summary of my work and a future perspective related to microfluidics and gene disruption/editing.

4.1 Conclusion

In this thesis, we report the first demonstration of lentiviral generation (LENGEN): packaging, production and transduction for gene disruption using digital microfluidics with an application of targeting the estrogen receptor alpha in a breast cancer cell line. First, we optimized electrode design on the DMF to cater for optimal generation of lentiviral titers and for the multiplexing of viral transduction analysis on-device. We characterized the integration of lentiviral generation with DMF by having a production area solely for the culture of producer cells, HEK293T, to package and produce lentiviruses based on the transfer vector of interest enabling us to choose between RNAi or CRISPR-Cas9 assays. Next, we did four serial dilutions to infect target cells where 24 hrs was found to be sufficient in terms of lentiviral titer obtained from the production area for perturbation to happen in gene expression. We then optimized and validated our system for transduction efficiency by assessing the expression mCherry through a heavy payload (plasmid ~15 kb) by transducing three different cell lines. We further tailored our LENGEN platform for directed gene silencing and gene editing using the RNAi and CRISPR-Cas9 system targeting the estrogen receptor alpha. Through these assays, we observed similar efficiencies to those acquired from benchtop experiments. To have a more complete workflow, we also applied LENGEN for directed knock out of an endogenously expressing fluorescent reporter (eGFP) in a non-small cell lung cancer cell line followed by downstream gene editing analysis (off-device). Overall, we were able to show the

versatility of the LENGEN platform by executing proof-of-principle validation of knockout/knockdown assays, at relative low cost, with small working volumes and material. To our knowledge, this platform is the first to be capable of automating the procedures of packaging, production and transduction with viral-derived vectors. We anticipate that this approach will greatly speed up (days instead of weeks) lentiviral production and transduction processes which can alleviate the tedium associated with optimizing lentiviral generation and transduction.

4.2 Future perspective

As the technology of DMF and other paradigms of microfluidics are developing, we believe that one day it will be possible to fully automate from the beginning to the end the whole workflow involved in gene editing. The tremendous utility of automation will provide the opportunity to reshape how we currently design, build, test, and learn gene-editing for different cell lines. Using microfluidics, it would be possible to build a next-generation automation gene editing platform that can obtain high gene delivery efficiencies, have a higher throughput and be able to execute parallel experiments.

In my opinion, a promising advancement will be to develop a fully automated machine learning platform that can run the whole pipeline of CRISPR gene editing or RNAi gene regulation based on a standard data set and proper experimental designs. The ideal platform will possess cloud-based data for the design of CRISPR (knock in, knock out, activation, repression) and RNAi strategies integrated with a system that assembles modular device pieces for each step of the pipeline (mentioned in Chapter 1.2: (1) to design and prepare the sh/sgRNA library, (2) to deliver the gene disruption machinery to the cell, (3) to analyze the results, and (4) to validate the gene perturbation) and the capacity for a

streamlined with feedback input/output performance. By doing so, the modularity will allow for the pipeline to be tailored to the researcher's application all while making the workflow simple by allowing the researcher to input all the necessary components into the platform which will produce an output of the edited and expanded cell line. For example, based on the researcher's desired method of delivery, there will be a choice between physical (i.e. electroporation), chemical transfections (lipofection, calcium phosphate transfection, etc.) or viral transduction methods with the option to deliver CRISPR machinery as ribonucleoproteins[88] or plasmids using LENGEN. Thus, this range of choice will permit for transient or stable expression of CRISPR components within easy to hard-to-transfect cell lines. Moreover, this next-generation automated platform is not limited to only to mammalian cells but is used with other organisms such as prokaryotic cells thanks to the low cost of fabrication for each modular microfluidic device. In this case, equipped with UV sterilization, cross-contamination can be completely avoided. For screening and selection, due to the modularity of the microfluidic devices, incorporation of optical fibers will serve as a way for sorting cells like FACs or impedance sensing can be done to select for healthy cells versus dead cells when selecting with an antibiotic resistance. Finally, having integrated sequencing in the platform will produce results within a quick time frame for researchers to assess their data. The whole pipeline will be based on standard data set and experimental designs and the machine learning will continuously update the analytical model, allowing the researcher to observe in real-time if each step was successfully completed for a conclusive edit. Thus, this platform will provide an easy and hands-free workflow of gene disruption for any researcher to use – giving everyone an opportunity to

engineer new cells to serve the greater good without having to go through the struggles of optimizing each step for successful gene disruption.

References

[1] a) Y. G. Kim, J. Cha, S. Chandrasegaran, *Proc Natl Acad Sci U S A* **1996**, *93*, 1156-1160; b) M. Bibikova, K. Beumer, J. K. Trautman, D. Carroll, *Science* **2003**, *300*, 764; c) M. Bibikova, M. Golic, K. G. Golic, D. Carroll, *Genetics* **2002**, *161*, 1169; d) A. J. Wood, T. W. Lo, B. Zeitler, C. S. Pickle, E. J. Ralston, A. H. Lee, R. Amora, J. C. Miller, E. Leung, X. Meng, L. Zhang, E. J. Rebar, P. D. Gregory, F. D. Urnov, B. J. Meyer, *Science* **2011**, *333*, 307.

[2] a) J. Boch, H. Scholze, S. Schornack, A. Landgraf, S. Hahn, S. Kay, T. Lahaye, A. Nickstadt, U. Bonas, *Science* **2009**, *326*, 1509-1512; b) M. J. Moscou, A. J. Bogdanove, *Science (New York, N.Y.)* **2009**, *326*, 1501; c) M. Christian, T. Cermak, E. L. Doyle, C. Schmidt, F. Zhang, A. Hummel, A. J. Bogdanove, D. F. Voytas, *Genetics* **2010**, *186*, 757-761; d) D. Reyon, S. Q. Tsai, C. Khayter, J. A. Foden, J. D. Sander, J. K. Joung, *Nat Biotechnol* **2012**, *30*, 460-465.

[3] a) M. Liu, S. Rehman, X. Tang, K. Gu, Q. Fan, D. Chen, W. Ma, *Frontiers in Genetics* **2019**, *9*; b) S. Hirotsune, H. Kiyonari, M. Jin, K. Kumamoto, K. Yoshida, M. Shinohara, H. Watanabe, A. Wynshaw-Boris, F. Matsuzaki, *Scientific Reports* **2020**, *10*; c) X.-D. Tang, F. Gao, M.-J. Liu, Q.-L. Fan, D.-K. Chen, W.-T. Ma, *Frontiers in Genetics* **2019**, *10*.

[4] a) L. Cong, F. A. Ran, D. Cox, S. Lin, R. Barretto, N. Habib, P. D. Hsu, X. Wu, W. Jiang, L. A. Marraffini, F. Zhang, *Science* **2013**, *339*, 819-823; b) X. Wu, D. A. Scott, A. J. Kriz, A. C. Chiu, P. D. Hsu, D. B. Dadon, A. W. Cheng, A. E. Trevino, S. Konermann, S. Chen, R. Jaenisch, F. Zhang, P. A. Sharp, *Nat Biotechnol* **2014**, *32*, 670-676; c) M. Jinek, A. East, A. Cheng, S. Lin, E. Ma, J. Doudna, *eLife* **2013**, *2*, e00471; d) L. A. Gilbert, M. H. Larson, L. Morsut, Z. Liu, G. A. Brar, S. E. Torres, N. Stern-Ginossar, O. Brandman, E. H. Whitehead, J. A. Doudna, W. A. Lim, J. S. Weissman, L. S. Qi, *Cell* **2013**, *154*, 442-451; e) M. L. Maeder, S. J. Linder, V. M. Cascio, Y. Fu, Q. H. Ho, J. K. Joung, *Nat Methods* **2013**, *10*, 977-979.

[5] a) X. Ma, X. Zhang, H. Liu, Z. Li, *Nature Plants* **2020**, *6*, 773-779; b) J. A. Doudna, E. Charpentier, *Science* **2014**, *346*, 1258096; c) P. D. Hsu, E. S. Lander, F. Zhang, *Cell* **2014**, *157*, 1262-1278; d) F. A. Ran, P. D. Hsu, C. Y. Lin, J. S. Gootenberg, S. Konermann, A. E. Trevino, D. A. Scott, A. Inoue, S. Matoba, Y. Zhang, F. Zhang, *Cell* **2013**, *154*, 1380-1389; e) O. Shalem, N. E. Sanjana, E. Hartenian, X. Shi, D. A. Scott, T. S. Mikkelsen, D. Heckl, B. L. Ebert, D. E. Root, J. G. Doench, F. Zhang, *Science* **2014**, *343*, 84-87.

[6] P. Bijoya, G. Montoya, *Biomedical Journal* **2020**, *43*, 8-17.

[7] A. Pickar-Oliver, C. A. Gersbach, *Nature Reviews Molecular Cell Biology* **2019**, 1.

[8] O. O. Abudayyeh, J. S. Gootenberg, P. Essletzbichler, S. Han, J. Joung, J. J. Belanto, V. Verdine, D. B. T. Cox, M. J. Kellner, A. Regev, E. S. Lander, D. F. Voytas, A. Y. Ting, F. Zhang, *Nature* **2017**, *550*, 280-284.

[9] M. M. Jore, M. Lundgren, E. Van Duijn, J. B. Bultema, E. R. Westra, S. P. Waghmare, B. Wiedenheft, Ü. Pul, R. Wurm, R. Wagner, M. R. Beijer, A.

Barendregt, K. Zhou, A. P. L. Snijders, M. J. Dickman, J. A. Doudna, E. J. Boekema, A. J. R. Heck, J. Van Der Oost, S. J. J. Brouns, *Nature Structural & Molecular Biology* **2011**, *18*, 529-536.

[10] a) L. A. Gilbert, M. A. Horlbeck, B. Adamson, J. E. Villalta, Y. Chen, E. H. Whitehead, C. Guimaraes, B. Panning, H. L. Ploegh, M. C. Bassik, L. S. Qi, M. Kampmann, J. S. Weissman, *Cell* **2014**, *159*, 647-661; b) A. A. Dominguez, W. A. Lim, L. S. Qi, *Nature Reviews Molecular Cell Biology* **2016**, *17*, 5-15.

[11] a) S. Baliou, M. Adamaki, A. M. Kyriakopoulos, D. A. Spandidos, M. Panayiotidis, I. Christodoulou, V. Zoumpourlis, *Int J Oncol* **2018**, *53*, 443-468; b) X. Xu, T. Wan, H. Xin, D. Li, H. Pan, J. Wu, Y. Ping, *The Journal of Gene Medicine* **2019**, *21*, e3107.

[12] a) T. Luo, L. Fan, R. Zhu, D. Sun, *Micromachines* **2019**, *10*; b) M. R. Javed, M. Noman, M. Shahid, T. Ahmed, M. Khurshid, M. H. Rashid, M. Ismail, M. Sadaf, F. Khan, *Microbiological Research* **2019**, *219*, 1-11; c) P. K. Sharma, M. Saharia, R. Srivstava, S. Kumar, L. Sahoo, *Frontiers in Marine Science* **2018**, *5*.

[13] T. A. O'Loughlin, L. A. Gilbert, *Annual Review of Cancer Biology* **2019**, *3*, 345-363.

[14] R. L. Setten, J. J. Rossi, S. P. Han, *Nature reviews. Drug discovery* **2019**, *18*, 421-446.

[15] RNAi video animation *Nature* **2011**.

[16] R. C. Wilson, J. A. Doudna, *Annual review of biophysics* **2013**, *42*, 217-239.

[17] N. Agrawal, P. V. N. Dasaradhi, A. Mohmmed, P. Malhotra, R. K. Bhatnagar, S. K. Mukherjee, *Microbiology and Molecular Biology Reviews* **2003**, *67*, 657-685.

[18] I. Smith, P. G. Greenside, T. Natoli, D. L. Lahr, D. Wadden, I. Tirosh, R. Narayan, D. E. Root, T. R. Golub, A. Subramanian, J. G. Doench, *PLOS Biology* **2017**, *15*, e2003213.

[19] M. Boettcher, M. T. McManus, *Molecular cell* **2015**, *58*, 575-585.

[20] a) N. E. Sanjana, O. Shalem, F. Zhang, *Nature Methods* **2014**, *11*, 783-784; b) O. Shalem, N. E. Sanjana, F. Zhang, *Nature Reviews Genetics* **2015**, *16*, 299-311; c) H. Koike-Yusa, Y. Li, E. P. Tan, M. D. C. Velasco-Herrera, K. Yusa, *Nature Biotechnology* **2014**, *32*, 267-273; d) A. Schuster, H. Erasimus, S. Fritah, P. V. Nazarov, E. van Dyck, S. P. Niclou, A. Golebiewska, *Trends in biotechnology* **2019**, *37*, 38-55.

[21] R. W. L. So, S. W. Chung, H. H. C. Lau, J. J. Watts, E. Gaudette, Z. A. M. Al-Azzawi, J. Bishay, L. T.-W. Lin, J. Joung, X. Wang, G. Schmitt-Ulms, *Molecular Neurodegeneration* **2019**, *14*.

[22] a) X. Tian, T. Gu, S. Patel, A. M. Bode, M.-H. Lee, Z. Dong, *npj Precision Oncology* **2019**, *3*, 1-8; b) F. A. Ran, P. D. Hsu, J. Wright, V. Agarwala, D. A. Scott, F. Zhang, *Nature Protocols* **2013**, *8*, 2281-2308.

[23] N. Hillson, M. Caddick, Y. Cai, J. A. Carrasco, M. W. Chang, N. C. Curach, D. J. Bell, R. Le Feuvre, D. C. Friedman, X. Fu, N. D. Gold, M. J. Herrgård, M. B. Holowko, J. R. Johnson, R. A. Johnson, J. D. Keasling, R. I. Kitney, A. Kondo, C. Liu, V. J. J. Martin, F. Menolascina, C. Ogino, N. J. Patron, M. Pavan, C. L. Poh, I. S. Pretorius, S. J. Rosser, N. S. Scrutton, M. Storch, H. Tekotte, E. Travnik, C. E. Vickers, W. S. Yew, Y. Yuan, H. Zhao, P. S. Freemont, *Nature Communications* **2019**, *10*, 2040.

[24] a) C. A. Lino, J. C. Harper, J. P. Carney, J. A. Timlin, *Drug Deliv* **2018**, *25*, 1234-1257; b) T. DiTommaso, J. M. Cole, L. Cassereau, J. A. Buggé, J. L. S. Hanson, D. T. Bridgen, B. D. Stokes, S. M. Loughhead, B. A. Beutel, J. B. Gilbert, K. Nussbaum, A. Sorrentino, J. Toggweiler, T. Schmidt, G. Gyuelveszi, H. Bernstein, A. Sharei, *Proceedings of the National Academy of Sciences* **2018**, *115*, E10907-E10914; c) C. Liu, L. Zhang, H. Liu, K. Cheng, *J Control Release* **2017**, *266*, 17-26; d) C. B. Moore, E. H. Guthrie, M. T.-H. Huang, D. J. Taxman, *Methods Mol Biol* **2010**, *629*, 141-158.

[25] K. Sliva, B. S. Schnierle, *Virology Journal* **2010**, *7*, 248.

[26] a) J. Cronin, X. Y. Zhang, J. Reiser, *Current gene therapy* **2005**, *5*, 387-398; b) L. Naldini, U. Blömer, P. Gallay, D. Ory, R. Mulligan, F. H. Gage, I. M. Verma, D. Trono, *Science* **1996**, *272*, 263-267; c) T. Dull, R. Zufferey, M. Kelly, R. J. Mandel, M. Nguyen, D. Trono, L. Naldini, *Journal of virology* **1998**, *72*, 8463-8471; d) R. Schlimgen, J. Howard, D. Wooley, M. Thompson, L. R. Baden, O. O. Yang, D. C. Christiani, G. Mostoslavsky, D. V. Diamond, E. G. Duane, K. Byers, T. Winters, J. A. Gelfand, G. Fujimoto, T. W. Hudson, J. M. Vyas, *Journal of Occupational & Environmental Medicine* **2016**, *58*, 1159-1166.

[27] H. E. Gouvarchin Ghaleh, M. Bolandian, R. Dorostkar, A. Jafari, M. F. Pour, *Biomedicine & Pharmacotherapy* **2020**, *128*, 110276.

[28] R. Zufferey, T. Dull, R. J. Mandel, A. Bukovsky, D. Quiroz, L. Naldini, D. Trono, *Journal of virology* **1998**, *72*, 9873-9880.

[29] M. Soldi, L. Sergi Sergi, G. Unali, T. Kerzel, I. Cuccovillo, P. Capasso, A. Annoni, M. Biffi, P. M. V. Rancoita, A. Cantore, A. Lombardo, L. Naldini, M. L. Squadrito, A. Kajaste-Rudnitski, *Molecular Therapy - Methods & Clinical Development* **2020**, *19*, 411-425.

[30] O. W. Merten, M. Hebben, C. Bovolenta, *Molecular therapy. Methods & clinical development* **2016**, *3*, 16017.

[31] a) H. Sinha, A. B. V. Quach, P. Q. N. Vo, S. C. C. Shih, *Lab on a Chip* **2018**, *18*, 2300-2312; b) A. H. C. Ng, M. D. Chamberlain, H. Situ, V. Lee, A. R. Wheeler, *Nature Communications* **2015**, *6*, 7513.

[32] K. F. Sonnen, C. A. Merten, *Developmental Cell* **2019**, *48*, 293-311.

[33] S.-S. Li, C.-M. Cheng, *Lab on a Chip* **2013**, *13*, 3782-3788.

[34] a) G. M. Whitesides, *Nature* **2006**, *442*, 368-373; b) D. Sugumar, L. Kong, in *Encyclopedia of Microfluidics and Nanofluidics* (Ed.: D. Li), Springer US, Boston, MA, **2008**, pp. 907-910.

[35] B. J. Kirby, *Micro- and Nanoscale Fluid Mechanics: Transport in Microfluidic Devices*, Cambridge University Press, **2010**.

[36] a) W. Qin, Y. He, J. Xiao, S. Liang, S. Wang, P. C. H. Li, Y. Sun, *Microfluidics and Nanofluidics* **2019**, *23*, 61; b) P. N. Nge, C. I. Rogers, A. T. Woolley, *Chemical Reviews* **2013**, *113*, 2550-2583.

[37] L. A. Low, C. Mummery, B. R. Berridge, C. P. Austin, D. A. Tagle, *Nature Reviews Drug Discovery* **2020**.

[38] a) A. Ramachandran, D. A. Huyke, E. Sharma, M. K. Sahoo, N. Banaei, B. A. Pinsky, J. G. Santiago, Cold Spring Harbor Laboratory, **2020**; b) R. Bruch, J. Baaske, C. Chatelle, M. Meirich, S. Madlener, W. Weber, C. Dincer, G. A. Urban, *Advanced Materials* **2019**, *31*, 1905311.

[39] F. Ahmadi, K. Samlali, P. Q. N. Vo, S. C. C. Shih, *Lab on a Chip* **2019**, *19*, 524-535.
[40] a) L. Shang, Y. Cheng, Y. Zhao, *Chemical Reviews* **2017**, *117*, 7964-8040; b) S.-Y. Teh, R. Lin, L.-H. Hung, A. P. Lee, *Lab on a Chip* **2008**, *8*, 198-220.
[41] S. Sohrabi, N. kassir, M. Keshavarz Moraveji, *RSC Advances* **2020**, *10*, 27560-27574.
[42] J.-C. Baret, O. J. Miller, V. Taly, M. Ryckelynck, A. El-Harrak, L. Frenz, C. Rick, M. L. Samuels, J. B. Hutchison, J. J. Agresti, D. R. Link, D. A. Weitz, A. D. Griffiths, *Lab on a Chip* **2009**, *9*, 1850-1858.
[43] Y. Zhu, Q. Fang, *Analytica Chimica Acta* **2013**, *787*, 24-35.
[44] S. Yazdian Kashani, A. Afzalian, F. Shirinichi, M. Keshavarz Moraveji, *RSC Advances* **2021**, *11*, 229-249.
[45] K. Samlali, F. Ahmadi, A. B. V. Quach, G. Soffer, S. C. C. Shih, *Small* **2020**, *16*.
[46] F. Mugele, J.-C. Baret, *Journal of Physics: Condensed Matter* **2005**, *17*, R705-R774.
[47] M. G. Pollack, A. D. Shenderov, R. B. Fair, *Lab Chip* **2002**, *2*, 96-101.
[48] K. Choi, A. H. C. Ng, R. Fobel, A. R. Wheeler, *Annual Review of Analytical Chemistry* **2012**, *5*, 413-440.
[49] S. H. Au, P. Kumar, A. R. Wheeler, *Langmuir : the ACS journal of surfaces and colloids* **2011**, *27*, 8586-8594.
[50] a) S. C. C. Shih, R. Fobel, P. Kumar, A. R. Wheeler, *Lab on a Chip* **2011**, *11*, 535-540; b) P. Q. N. Vo, M. C. Husser, F. Ahmadi, H. Sinha, S. C. C. Shih, *Lab on a Chip* **2017**, *17*, 3437-3446; c) M. C. Husser, P. Q. N. Vo, H. Sinha, F. Ahmadi, S. C. C. Shih, *ACS synthetic biology* **2018**, *7*, 933-944; d) E. Moazami, J. M. Perry, G. Soffer, M. C. Husser, S. C. C. Shih, *Analytical Chemistry* **2019**, *91*, 5159-5168.
[51] a) V. Srinivasan, V. K. Pamula, R. B. Fair, *Lab Chip* **2004**, *4*, 310-315; b) H. Yang, V. N. Luk, M. Abelgawad, I. Barbulovic-Nad, A. R. Wheeler, *Analytical Chemistry* **2009**, *81*, 1061-1067.
[52] H. Geng, S. K. Cho, *Lab on a Chip* **2019**, *19*, 2275-2283.
[53] J. Zhou, L. Lu, K. Byrapogu, D. M. Wootton, P. I. Lelkes, R. Fair, *Virtual and Physical Prototyping* **2007**, *2*, 217-223.
[54] I. Barbulovic-Nad, H. Yang, P. S. Park, A. R. Wheeler, *Lab on a Chip* **2008**, *8*, 519-526.
[55] I. Barbulovic-Nad, S. H. Au, A. R. Wheeler, *Lab on a Chip* **2010**, *10*, 1536-1542.
[56] I. A. Eydelnant, U. Uddayasankar, B. B. Li, M. W. Liao, A. R. Wheeler, *Lab on a Chip* **2012**, *12*, 750-757.
[57] a) A. C. Madison, M. W. Royal, F. Vigneault, L. Chen, P. B. Griffin, M. Horowitz, G. M. Church, R. B. Fair, *ACS Synth Biol* **2017**, *6*, 1701-1709; b) X. Li, M. Aghaamoo, S. Liu, D.-H. Lee, A. P. Lee, *Small* **2018**, *14*, 1802055; c) A. Sharei, J. Zoldan, A. Adamo, W. Y. Sim, N. Cho, E. Jackson, S. Mao, S. Schneider, M. J. Han, A. Lytton-Jean, P. A. Basto, S. Jhunjhunwala, J. Lee, D. A. Heller, J. W. Kang, G. C. Hartoularos, K. S. Kim, D. G. Anderson, R. Langer, K. F. Jensen, *Proceedings of the National Academy of Sciences* **2013**, *110*, 2082-2087; d) X. Han, Z. Liu, M. c. Jo, K. Zhang, Y. Li, Z. Zeng, N. Li, Y. Zu, L. Qin, *Science Advances* **2015**, *1*, e1500454.

[58] a) R. Tran, D. R. Myers, J. E. Shields, B. Ahn, Y. Qiu, C. Hansen, Y. Sakurai, R. Moot, H. T. Spencer, C. B. Doering, W. A. Lam, *Blood* **2015**, *126*; b) R. Tran, D. R. Myers, G. Denning, J. E. Shields, A. M. Lytle, H. Alrowais, Y. Qiu, Y. Sakurai, W. C. Li, O. Brand, J. M. Le Doux, H. T. Spencer, C. B. Doering, W. A. Lam, *Molecular Therapy* **2017**, *25*, 2372-2382.
[59] N. Moore, J. R. Chevillet, L. J. Healey, C. McBrine, D. Doty, J. Santos, B. Teece, J. Truslow, V. Mott, P. Hsi, V. Tandon, J. T. Borenstein, J. Balestrini, K. Kotz, *Scientific Reports* **2019**, *9*, 15101.
[60] K. P. Gill, M. Denham, *Current Protocols in Molecular Biology* **2020**, *133*, e125.
[61] N. Drayman, A. Oppenheim, *Current Protocols in Cell Biology* **2011**, *51*, 26.11.21-26.11.27.
[62] M. J. Li, J. J. Rossi, *CSH protocols* **2007**, *2007*, pdb.prot4755.
[63] a) M. C. Milone, U. O'Doherty, *Leukemia* **2018**, *32*, 1529-1541; b) H. Hayashi, Y. Kubo, M. Izumida, T. Matsuyama, *Scientific Reports* **2020**, *10*, 21474.
[64] L. M. Y. Leclerc, G. Soffer, D. H. Kwan, S. C. C. Shih, *Biomicrofluidics* **2019**, *13*, 034106.
[65] S. Anderson, B. Hadwen, C. Brown, *Lab on a Chip* **2021**, *21*, 962-975.
[66] H. Erfle, B. Neumann, U. Liebel, P. Rogers, M. Held, T. Walter, J. Ellenberg, R. Pepperkok, *Nature Protocols* **2007**, *2*, 392-399.
[67] E. A. Saunderson, P. Stepper, J. J. Gomm, L. Hoa, A. Morgan, M. D. Allen, J. L. Jones, J. G. Gribben, T. P. Jurkowski, G. Ficz, *Nature Communications* **2017**, *8*, 1450.
[68] S. Vijayraghavan, B. Kantor, *J Vis Exp* **2017**, 56915.
[69] F. Cao, X. Xie, T. Gollan, L. Zhao, K. Narsinh, R. J. Lee, J. C. Wu, *Mol Imaging Biol* **2010**, *12*, 15-24.
[70] A. N. Aznan, N. Abdul Karim, W. Z. Wan Ngah, Z. Jubri, *Oncol Lett* **2018**, *16*, 73-82.
[71] a) L. Y. Brown, W. Dong, B. Kantor, *STAR protocols* **2020**, *1*, 100152; b) A. McCarron, M. Donnelley, D. Parsons, *Cell & Gene Therapy Insights* **2017**, *3*.
[72] a) P. L. Sinn, S. L. Sauter, P. B. McCray, *Gene Therapy* **2005**, *12*, 1089-1098; b) J. R. Counsell, Z. Asgarian, J. Meng, V. Ferrer, C. A. Vink, S. J. Howe, S. N. Waddington, A. J. Thrasher, F. Muntoni, J. E. Morgan, O. Danos, *Scientific Reports* **2017**, *7*, 44775.
[73] S. Wotherspoon, A. Dolnikov, G. Symonds, R. Nordon, *Journal of virology* **2004**, *78*, 5097-5102.
[74] a) A. C. Pirona, R. Oktriani, M. Boettcher, J. D. Hoheisel, *Biology Methods and Protocols* **2020**, *5*; b) W. C. Hines, P. Yaswen, M. J. Bissell, *Nature Communications* **2015**, *6*, 6927.
[75] *Human gene therapy* **2001**, *12*, 1893-1905.
[76] B. L. Ellis, M. L. Hirsch, J. C. Barker, J. P. Connelly, R. J. Steininger, M. H. Porteus, *Virology Journal* **2013**, *10*, 74.
[77] a) R. L. Klein, R. D. Dayton, J. B. Tatom, K. M. Henderson, P. P. Henning, *Molecular Therapy* **2008**, *16*, 89-96; b) M. L. Hirsch, B. M. Fagan, R. Dumitru, J. J. Bower, S. Yadav, M. H. Porteus, L. H. Pevny, R. J. Samulski, *PLOS ONE* **2011**, *6*, e27520.

[78] T. Traboulsi, M. El Ezzy, J. L. Gleason, S. Mader, *Journal of Molecular Endocrinology* **2017**, *58*, R15-R31.
[79] T. Xiao, W. Li, X. Wang, H. Xu, J. Yang, Q. Wu, Y. Huang, J. Geradts, P. Jiang, T. Fei, D. Chi, C. Zang, Q. Liao, J. Rennhack, E. Andrechek, N. Li, S. Detre, M. Dowsett, R. M. Jeselsohn, X. S. Liu, M. Brown, *Proceedings of the National Academy of Sciences* **2018**, *115*, 7869-7878.
[80] G. Van Peer, P. Mestdagh, J. Vandesompele, *Scientific reports* **2012**, *2*, 222-222.
[81] S. C. Taylor, K. Nadeau, M. Abbasi, C. Lachance, M. Nguyen, J. Fenrich, *Trends in Biotechnology* **2019**, *37*, 761-774.
[82] a) H. Li, Y. Yang, W. Hong, M. Huang, M. Wu, X. Zhao, *Signal Transduction and Targeted Therapy* **2020**, *5*, 1; b) B. Liu, A. Saber, H. J. Haisma, *Drug Discovery Today* **2019**, *24*, 955-970.
[83] S. Alimperti, P. Lei, J. Tian, S. T. Andreadis, *Gene Therapy* **2012**, *19*, 1123-1132.
[84] X. Xu, D. Gao, P. Wang, J. Chen, J. Ruan, J. Xu, X. Xia, *Scientific Reports* **2018**, *8*, 11649.
[85] a) X. Han, Z. Liu, Y. Ma, K. Zhang, L. Qin, *Advanced Biosystems* **2017**, *1*, 1600007; b) X. Han, Z. Liu, L. Zhao, F. Wang, Y. Yu, J. Yang, R. Chen, L. Qin, *Angewandte Chemie International Edition* **2016**, *55*, 8561-8565.
[86] Y. Xing, Y. Liu, R. Chen, Y. Li, C. Zhang, Y. Jiang, Y. Lu, B. Lin, P. Chen, R. Tian, X. Liu, X. Cheng, *Lab on a Chip* **2021**, *21*, 1886-1896.
[87] A. P. Manceur, H. Kim, V. Misic, N. Andreev, J. Dorion-Thibaudeau, S. Lanthier, A. Bernier, S. Tremblay, A.-M. Gélinas, S. Broussau, R. Gilbert, S. Ansorge, *Hum Gene Ther Methods* **2017**, *28*, 330-339.
[88] J. R. Hamilton, C. A. Tsuchida, D. N. Nguyen, B. R. Shy, E. R. McGarrigle, C. R. Sandoval Espinoza, D. Carr, F. Blaeschke, A. Marson, J. A. Doudna, *Cell Reports* **2021**, *35*, 109207.

Appendix: Supplementary information

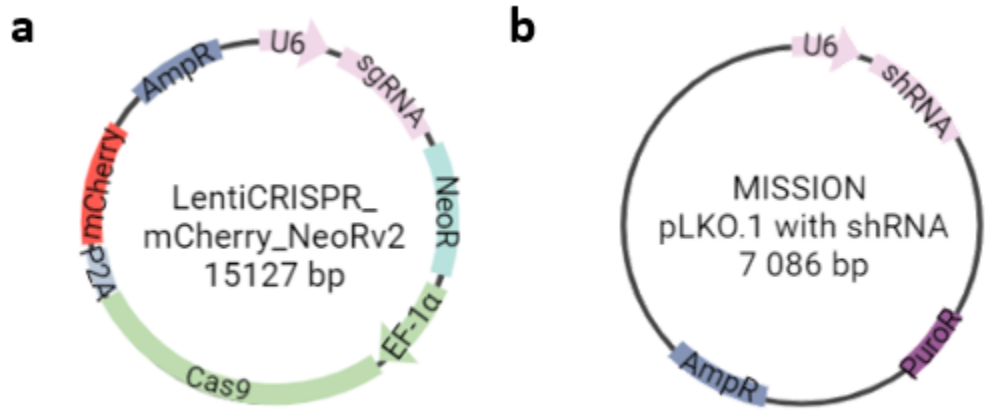

Figure S1 - Transfer plasmids used in this study. *(a) LentiCRISPR_mCherry_NeoRv2 (LCMNv2) is a viral transfer vector that contains an sgRNA (targeting either eGFP or ESR1) under the promoter U6 and a spCas9 gene cassette linked to a fluorescent reporter, mCherry, via a P2A linker which are all under the promoter EF-1α. A neomycin/kanamycin resistance was assembled into the plasmid. (b) MISSION® pLKO.1 constructs contain an shRNA targeting ESR1 under the promoter of U6 and has a puromycin resistance cassette. The first plasmid is deposited into the online Addgene repository (Cambridge, MA).*

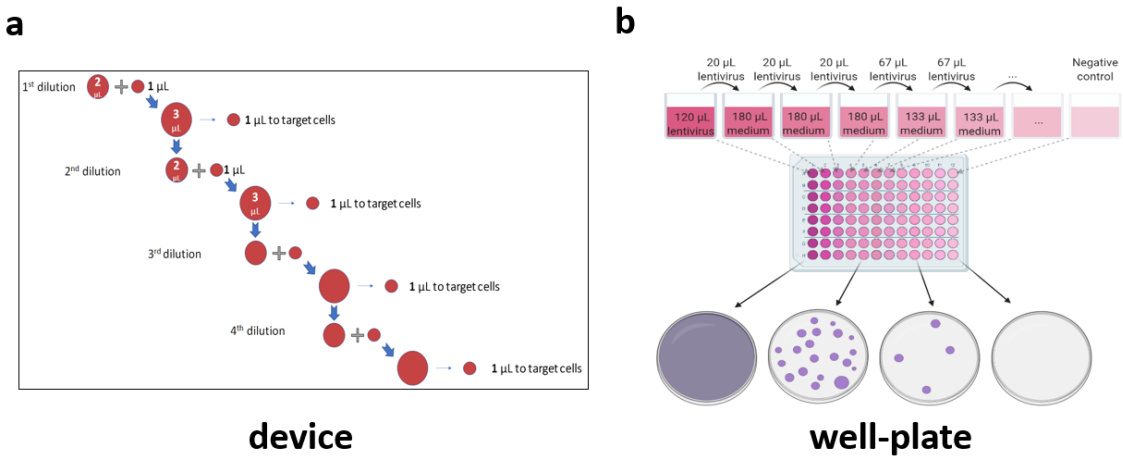

Figure S2 - Lentiviral transduction dilutions to measure mean viral titer in the device and well-plate. *(a) Serial dilutions of 1:3, 1:6, 1:12, and 1:24 of lentiviral supernatant are formed at the production area following a dilution protocol. Each 1 µL unit DMEM droplet is applied to HEK293T cells in a serial fashion. A dilution of 1:3 (DMEM and viral titers) was implemented by merging 1 µL of DMEM with 2 µL of the supernatant containing the viruses. 1 µL of the merged product was split and actuated to a 'target cell' region while the remainder (2 µL) was saved for other dilutions. This procedure was repeated three times to generate dilutions 1:6, 1:12, and 1:24. After monitoring for two days, it is possible to infer the viral titer via the fluorescence of target cells based on equation 1. (b) Serial dilutions of lentiviruses are applied to HEK293T cells in a 96-well plate. Colonies were allowed to grow in the presence of the puromycin for 7-8 days with medium renewal each 2 days and stained with 0.1 % w/v crystal violet in 20% ethanol and counted when the negative control well was completely dead. Counted colonies were converted into transducing units per mL via equation 2 shown in the methodology.*

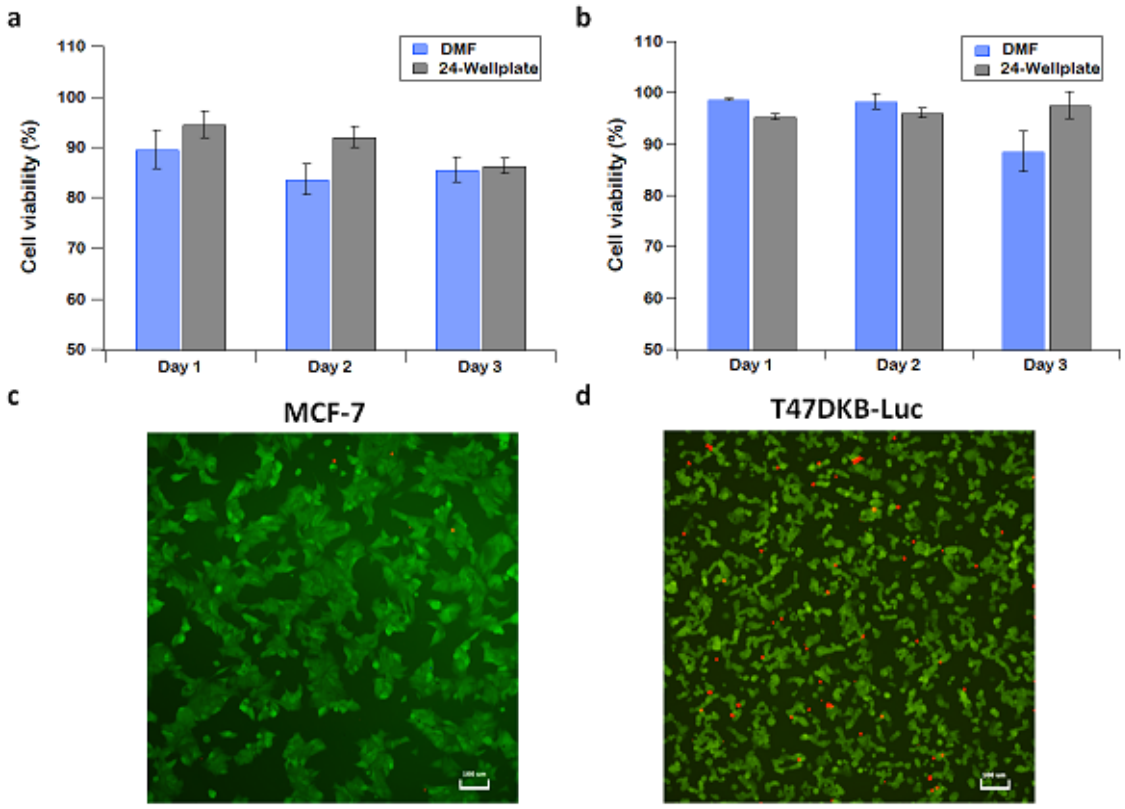

Figure S3 - Cell viability of breast cancer cells' (MCF-7 & T47DKB-Luc) on DMF and 24-wellplate throughout 3 days. *(a-b) Viability bar graph of MCF-7 and T47DKB-Luc cells. Cell viability data was measured (as seen in section 2.10) via Hoechst 33342 staining of the nuclei and FDA/PI staining for live and dead cells . (c-d) Qualitative images of cell viability for breast cancer cells stained with FDA/PI in 24-well plate after 3 days.*

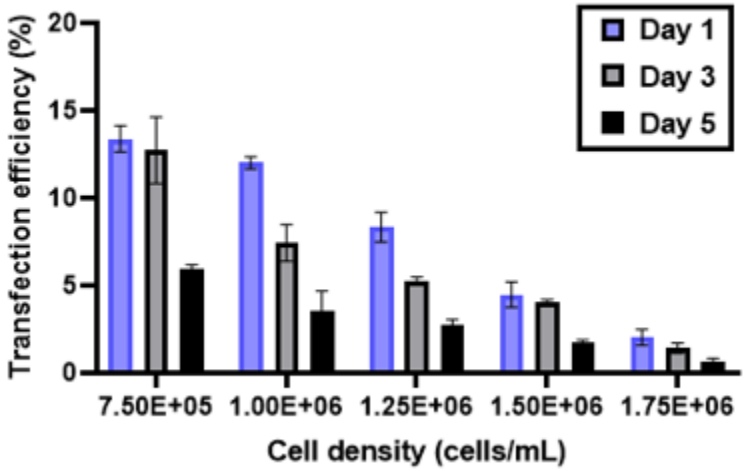

Figure S4 - Lipid-mediated transfection efficiency of T47DKB-Luc with plasmid eGFP-N1 in 24-wellplate over 5 days. *Different cell densities were seeded in a well-plate for evaluation of transfection efficiency based on the observation of eGFP fluorescence in T47DKB-Luc cells. 750 ng of DNA plasmid was transfected into the cells. Within the first day the highest transfection efficiency seen at the lowest cell density is ~ 13.4% and decreases over the 5 days. The highest cell density was observed to reach the lowest transfection efficiencies.*

Sample calculations:

For dilution 1:3 on microscale, seeding density is 3 x 10^6 cells/mL with an average viral titer of 3.68 x 10^6 TU/mL after **24 hours**

$$\frac{3.68 \times 10^6\ TU/mL}{3 \times 10^6\ cells/ml} \approx 1.23\ TU\ per\ cell$$

For dilution 1:3 on microscale, seeding density is 3 x 10^6 cells/mL with an average viral titer of 1.05 x 10^7 TU/mL after **48 hours**

$$\frac{1.05 \times 10^7\ TU/mL}{3 \times 10^6\ cells/ml} \approx 3.55\ TU\ per\ cell$$

For dilution 3:10 on macroscale, seeding density is 5 x 10^6 cells/mL with an average viral titer of 1.4 x10^7 TU/mL after **5 days** of harvesting

$$\frac{1.4 \times 10^7 TU/mL}{5 \times 10^6 cells/ml} \approx 2.81\ TU\ per\ cell$$

Figure S5 – Sample calculations for measuring the transducing units packaged per producer cell. *The cell seeding density was divided by the obtained mean viral titer to calculate the approximate transducing units packaged per producer cell on macroscale and microscale. The mean viral titer is obtained through plots in Figure 3.4c.*

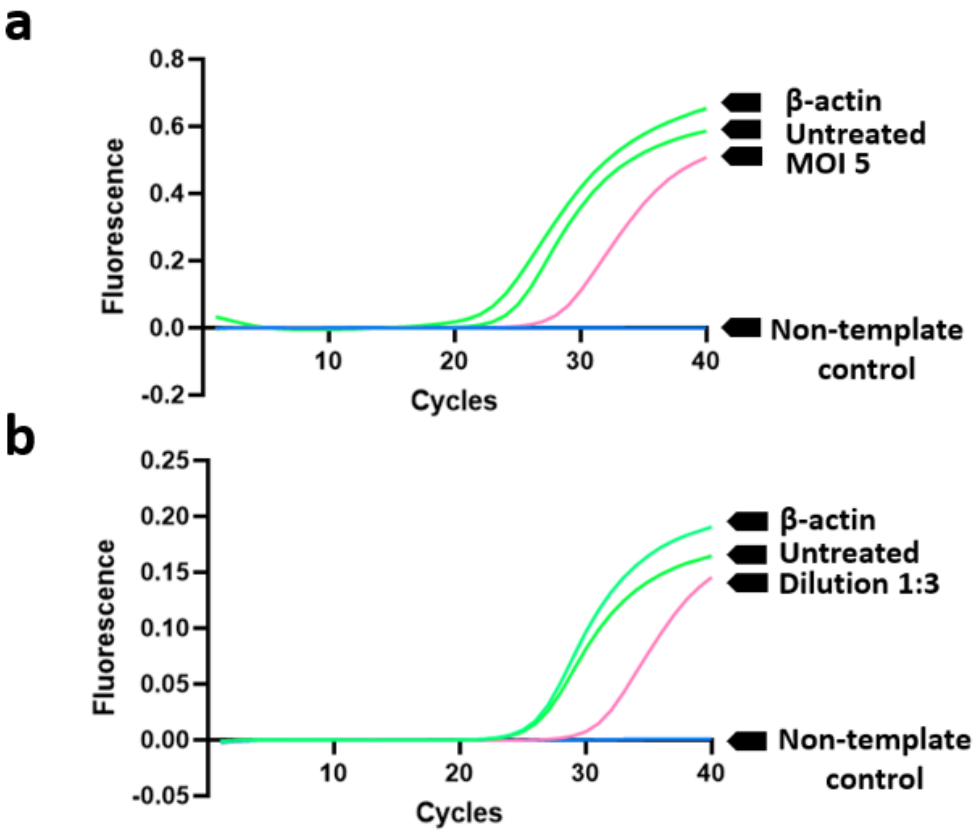

Figure S6 - RT-qPCR raw data examples: RNAi assay on MCF-7's on LENGEN and in a 96-well plate. *(a) Amplification plots measuring gene expression of ESR1 and ACTB (as a reference gene) in MCF-7 cells on LENGEN. Pooled 1:3 dilutions were transferred into a well-plate and grown with antibiotic for seven days. (b) Amplification plots measuring gene expression of ESR1 and ACTB (as a reference gene) in MCF-7 cells. MCF-7 cells were treated with viral particles containing shRNA constructs in a 96-well plate and selected with antibiotic for seven days.*

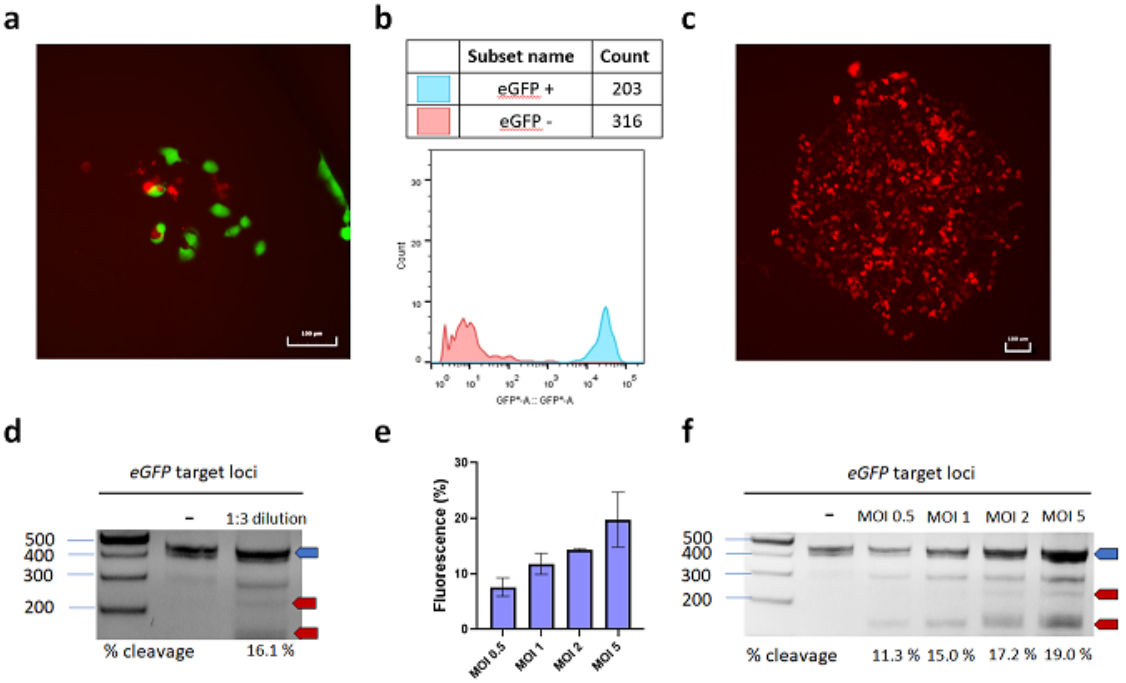

Figure S7 - Expansion of eGFP knockout cells transduced on LENGEN and knockout assays for eGFP on device and in well-plate. *(a) Pooled dilutions (1:3) of H1299 into a 96-well plate. Overlay images of mCherry and eGFP images show the knockout of eGFP in some cells 5 days post-transduction. (b) Cell sorting of H1299 grown from pooled dilutions (1:3). Flow cytometry data showing the count of eGFP knockout cells versus (+)eGFP cells. (c) Single cell expansion of (-)eGFP/(+)mCherry H1299 cells. The heterogenous population was cell sorted for single cell expansion of eGFP knocked out and integrated mCherry-expressing cells. The cells were further expanded for establishment of a new endogenously expressing fluorescent cell line. (d) Evaluating the knockout efficiency of eGFP in H1299 cells with lentiviral particles containing all-in-one Cas9/sgRNA targeting eGFP. Genomic cleavage assay done after seven days post-transduction on the pooled 1:3 dilution performed on LENGEN. The wildtype band is 433 bp (shown by the blue arrow arrow) and the expected cleavage bands are 293 bp and 160 bp (shown by the red arrows arrow). There is presence of un-specific bands (~400 bp and ~310 bp) due to many repeated sequences located near the target loci. (e) Plot of fluorescence percentages at different MOIs (0.5, 1, 2 and 5) were measured in H1299 cells, two days post-transduction in a 96-well plate. (f) Genomic cleavage assay done after seven days post-transduction on each interrogated MOI performed in well-plates assessing the eGFP target loci. Error bars for both plots represent ± 1 S.D. with N = 3.*